GRS

Sealing Capacity of a
Seal System in Rock Salt
– Hydraulic Impact of
the EDZ Long-term
Evolution

GRS

Sealing Capacity of a Seal System in Rock Salt – Hydraulic Impact of the EDZ Long-term Evolution

Oliver Czaikowski
Jürgen Dittrich
Larissa Friedenberg
Uwe Hertes
Kyra Jantschik
Michael Komischke
Klaus Wieczorek
Bernd Zehle

November 2018

Abstract

GRS is investigating sealing and backfilling materials planned to be utilized in a nuclear repository in a salt formation. The program aims at providing experimental data needed for the theoretical analysis of the long-term sealing capacity of the seal system, including the closing of the contact seam and the recovery of the excavation damaged zone (EDZ) under load and dry or wet conditions. The interaction with sealing materials is simulated in laboratory tests by using hollow cylinders of salt equipped with a central concrete seal in isostatic cells. Experimental investigations on the long-term re-compaction behavior of the sealing system, under partial or near-full brine saturation, are performed. First results showed that the method is able to fulfil the expectations of providing useful data for long-term predictive calculations. In addition, some first numerical calculations have been performed, based on former calibration work and focusing on the simulation of the contact zone evolution. This report resumes the discussion on reduction of permeability resulting from mechanical closure by creeping of salt, which is accelerated in the presence of solution, or by chemical reactions.

Acknowledgements

Table of Contents

1   Introduction

On behalf of the German Ministry for Economic Affairs and Energy (Bundesministerium für Wirtschaft und Energie, BMWi), GRS performs application-oriented safety research related to radioactive waste management in Germany. Among others, GRS is investigating sealing and backfilling materials planned to be utilized in a repository in a salt formation.

The German safety requirements for a repository of heat-generating nuclear waste /BMU 10/ comprise several safety principles, the most important ones being:

- Radionuclides and other contaminants in the waste must be concentrated and contained in a containment-providing rock zone (CRZ) and thus be isolated from the biosphere as long as possible.

- Waste disposal must ensure that release of radionuclides from the repository enhances only insignificantly the risks resulting from natural radiation exposure.

A robust barrier system is required to ensure that the safety principles are met. The most important barrier in a repository in rock salt is the salt formation itself. Natural rock salt exhibits a very low permeability (below 10^{-22} m^2 for undisturbed salt) and a pronounced visco-plastic deformation behavior which causes the closure of voids with time under compressive stress states. According to the current concept, remaining voids in the repository are backfilled during and after waste emplacement with crushed salt which is expected to be compacted with time to a material exhibiting properties similar to the formation. Until this is achieved, however, geotechnical barriers have to ensure the containment of the waste. Several concepts for drift and shaft seals are under development, considering components consisting of MgO and cement based salt concrete. Integral permeability values of $5 \cdot 10^{-17}$ m^2 are assumed for the individual seal components /MÜL 12/.

During mining, the rock close to the excavation experiences highly inhomogeneous stress states leading to micro-fracturing that causes volume increase (dilatancy). This damaged rock zone (herein after referred to as the excavation damaged zone (EDZ)) can exhibit permeability several orders of magnitude higher than the undisturbed rock. Permeability values up to the order of 10^{-14} m^2 have been measured /BEC 04/, /JOC 08/. EDZ permeability will reduce with time when, due to creep of the rock salt onto a load-bearing seal structure, a compressive stress state is established and the EDZ recovers.

Since the performance of seals in a rock salt repository is determined by the interaction with the surrounding rock, it is necessary to investigate the system of seal element and rock salt. The critical issue is the recovery of the EDZ. The time scale of recovery will be influenced by the pore fluid. It is known that rock salt deforms more readily in the presence of moisture because pressure solution and redeposition processes are operative. Therefore, a partial saturation of pore space may result in a much faster EDZ recovery. On the other hand, at full saturation a positive pore pressure might develop which reduces compressive stress and hinders recompaction of dilated salt.

So, with respect to EDZ evolution, the following three scenarios are conceivable:

  i.   There is no contact between the EDZ and brine/vapor,

  ii.   There is brine/vapor flow into the sealing system, as a result the EDZ pore space will be partially saturated,

  iii. The EDZ or/and the sealing system is nearly fully saturated, as a result to viscous deformation processes positive pore pressures can evolve.

While there is extensive knowledge existing in Germany on long-term rock salt behavior /WIE 10/ for the dry case (i), the material behavior of rock salt in contact with moisture/brine is only known qualitatively. What is missing here is a clear database coming from well-defined experimental investigations on the long-term

recompaction behavior of damaged rock salt itself and in interaction with the seal system, featuring the presence of moisture/brine according to case (ii) and (iii).

In order to demonstrate hydro-mechanical material stability under representative load scenarios, the impact of the EDZ and the sealing capacity of the seal system, a comprehensive laboratory testing program is carried out related to FKZ 02E11243 and /DOP 12/, /CZA 16/ and /JAN 18a/. The focus of the work is not on the observation of the saturation process and the derivation of two-phase flow parameters, but on a systematic investigation of the material behavior leading to EDZ recompaction and closure of a potentially conductive contact seam. It is meant to result in a set of material parameters needed to treat the process in a numerical way.

2 Theoretical background

2.1 Sealing model for integrated assessment

The detail of the representation of sealing structures in integrated performance assessment differs in the different national programs. The long-term safety assessment for high level waste in salt in Germany so far used approaches regarding the seals as quasi homogenous elements. In this approach, the fluid flow through seals is calculated by using an averaged permeability value over the whole cross-section of the seal section including contact seam, and excavation damaged zone. The permeability value is constant in time and conservative values are used to include special processes like EDZ or material alterations with time. More severe changes in permeability are taken into account by changing the permeability stepwise in time. This approach has also been used in the simulations for the VSG, /LAR 13/.

In /RÜB 16/ a mathematical model has been defined to overcome the limitations of the use of averaged permeabilities in integrated safety assessment and by this reduce conservatisms in the simulations. Two effects are to be considered in more detail, making the permeability a function of time.

The first effect is the existence of an EDZ. The EDZ develops around excavations during the construction of the mine due to stress release. Most of the EDZ around seal locations is removed by means of mining technique before seal construction. However, part of the EDZ often cannot be removed or is quickly redeveloping during the time between EDZ removal and seal construction. This damaged zone around the drift section where the seal is constructed has an increased permeability and extends up to several tens of centimeters into the rock.

The second effect to be considered is the degradation of the sealing material by corroding fluids flowing through the seal. In most cases, the sealing material is not in chemical equilibrium with the brine streaming in. This is the case, for instance, when MgCl-based concrete material is used for a seal which is flown through by a sodium chlorine brine (or a NaCl-based concrete material which is

streamed by a magnesium chlorine solution) resulting in a dissolution of minerals and precipitation of others. The permeability of the corroded material is typically higher than that of the initially used material. Due to the low permeability of the seal, the corrosion process occurs within a sharp corrosion front slowly progressing through the seal.

This resistance can be used to calculate the effective seal permeability for a seal divided in different regions with different permeabilities using the well-known laws for serial and parallel connection of resistances, Fig. 2.1.
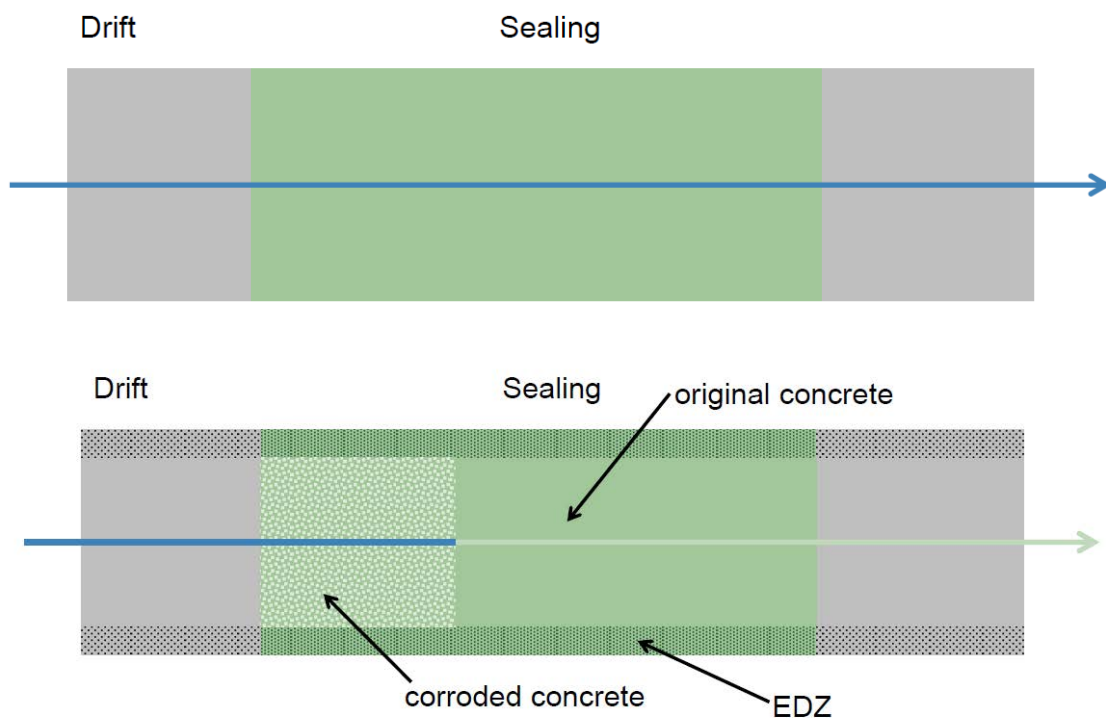
Fig. 2.1   Homogenous sealing structure in integrated model (above) and different compartments of the seal (below), /RÜB 16/

Subsequently, the seal is divided into three spatial separated compartments: (i) original concrete material, (ii) corroded concrete material and (iii) EDZ. The contact seam is not considered in this approach.

The total resistance of the seal can be calculated at each point in time from the fractional resistances of the individual compartments. It has to be noted, however, that due to the dependence of the resistance on the viscosity of the fluid, the

resistance of a compartment might change over time just due to changes in fluid composition.

2.2 Example of a sealing element in rock salt

The influences on a sealing element of the two processes EDZ-closure and cement corrosion are illustrated by an exemplary calculation using a seal of 30 m in length with an initial permeability of the sealing core made from salt concrete material of $5 \cdot 10^{-19}$ m^2. The EDZ around the sealing radially extends 1 m into the rock and has an initial permeability of $4.5 \cdot 10^{-17}$ m^2. Brine is flowing in at a pressure of 10 MPa. The results of the simulation, in terms of hydraulic resistance over time, are shown in Fig. 2.2. The black solid line denotes the resulting effective parameters across the entire cross section of the sealing, while the dashed lines show the same parameters, but distinguish between the concrete core of the seal and the EDZ in the host rock around the seal.

As is shown in Fig. 2.2, the hydraulic resistance of the sealing is dominated at the beginning by the comparatively low resistance of the EDZ. The EDZ is then re-compacting with time and the resistance of the EDZ is increasing during the first 300 to 400 years by one order of magnitude. After about 500 years, the hydraulic resistance of the EDZ exceeds those of the sealing core, which dominates the resistance of the sealing thereafter. The hydraulic resistance of the sealing concrete core is nearly constant for nearly one thousand years. An alteration process along the contact seam could not be considered by this approach.

The integrated amount of brine inflow is also plotted in Fig. 2.2. After one thousand years, the resistance is slowly decreasing due to the progressing corrosion process but does not change more than a factor of two until about ten thousand years. The integrated total amount of brine inflow until the complete corrosion of the seal is about 1500 m^3.

After about 13000 years, the hydraulic resistance is rapidly decreasing and reaches its minimum value after about 15300 years. After this point of time, the

integrated amount of brine inflow increases rather quickly above one million cubic meters.
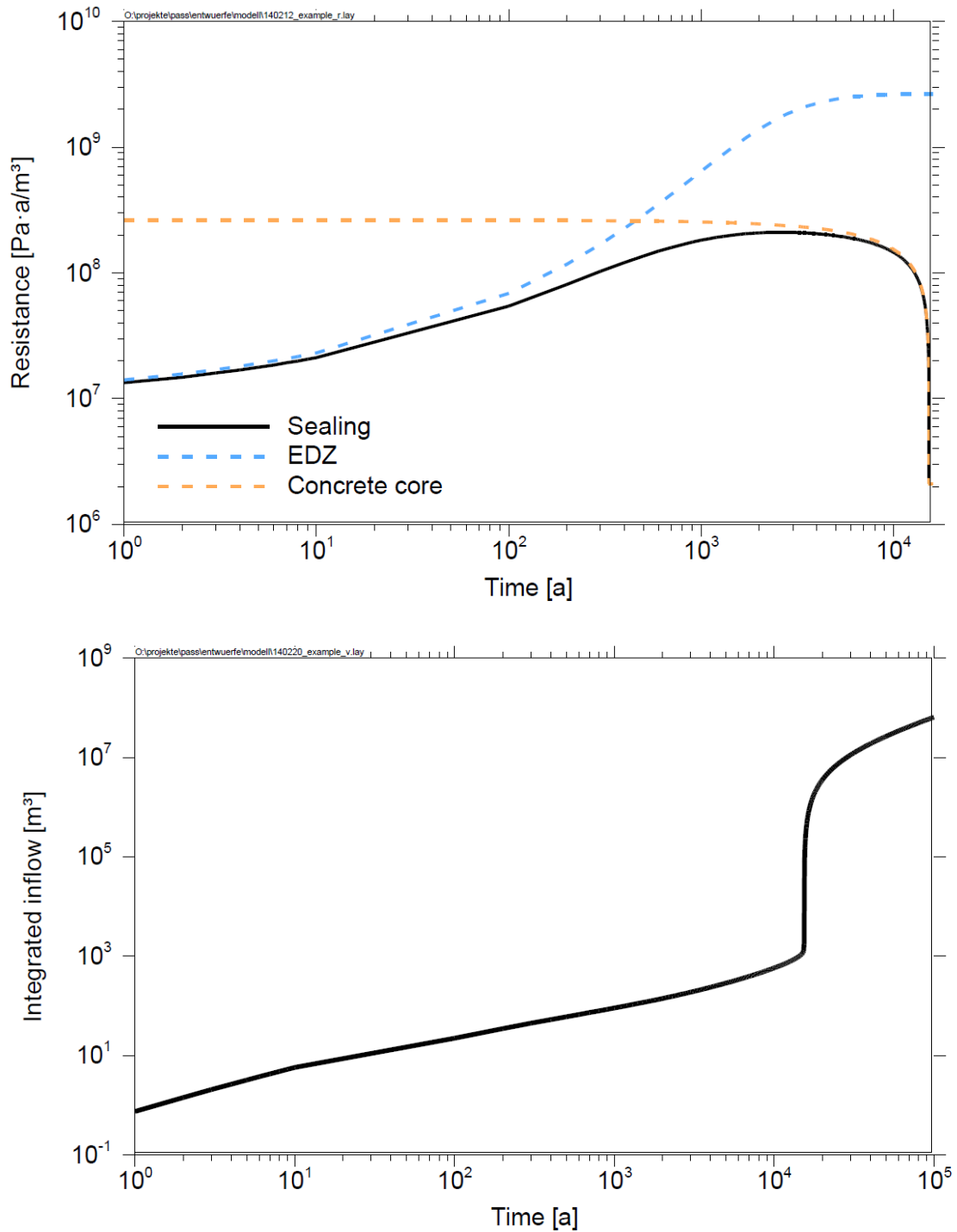

Fig. 2.2   Hydraulic resistance of a seal, its concrete core and the EDZ around the seal versus time (above), Integrated inflow through sealing versus time (below), /RÜB 16/

2.3   Discussion

It has to be noted that this is only an exemplary result which is highly sensitive to the input parameters. /RÜB 16/ shows some deterministic parameter variation where one parameter has been changed compared to the reference parameters in each calculation.

One of the largest deviations compared to the reference case comes from the change of the seal length. An increased sealing length by a factor of two results in a time needed to fully corrode the sealing which is increased by a factor of four. A change of the corroded seal permeability does not change the corrosion behaviour in a significant way before the seal has been completely corroded. As long as there is a non-corroded part of the seal, the seal behaviour is dominated by this part. Changing the corrosion capacity does linearly change the time needed to fully corrode the sealing but does not change integrated inflow curve for times before the sealing is fully corroded.

Changing the EDZ behaviour can significantly affect the amount of brine flowing through the seal. This was tested by changing the extension of the EDZ into the host rock and the fitting parameter resulting in a delay by a factor of five to close the EDZ. This finding supports the assumption that the contact seam as being the primary path way for solutions and its recompaction behaviour with time, is of great importance to the sealing behaviour of the whole sealing structure.

Therefore, GRS performs experiments on the hydraulic resistivity measurements of a system consisting of a salt concrete seal element and the surrounding dilated rock salt at the laboratory scale for systematic investigation of the material behavior leading to pathway reduction.

3 Experimental investigations

3.1 Setup of advection experiments

Advection experiments aim at investigating the advective flow and its impact on the corrosions processes and development of permeability. Based on the Darcy's law for compressible fluids the permeability K can be calculated according to

$$k = \frac{Q \cdot \eta \cdot p_1 \cdot L}{\Delta p \cdot p^* \cdot A}$$

(3.1)

k is the permeability in [m^2], Q the volume flow in [m^3/s], η the dynamic viscosity of the solution in [kg/(m·s)], p_1 the gas pressure at the outflowing surface in [kg/(m·s^2)], p_2 the gas pressure at the inflowing surface in [kg/(m·s^2)], L the length of the sample in [m], Δp the difference pressure (p_2-p_1) in [kg/(m·s^2)], p^* the average internal pressure in the pores ((p_1+p_2)/2) in [kg/(m·s^2)] and A the cross section area of the sample in [m^2].

Additionally, the collected solution is analysed with regard to its composition, development of density and pH-value.

The advection experiments are divided in two types of samples:

a) pure dilated rock salt samples

b) combined samples of salt concrete fitted into hollow cylinders of dilated rock salt

For performing experiments on the system consisting of a salt concrete seal element and the surrounding dilated rock salt at the laboratory scale, the idea is to use hollow salt cylinders furnished with a central core of salt concrete which are placed in isostatic cells to impose confining stress. Thus, a combined sample represents the system of seal element, contact seam and surrounding rock at a small scale.

The salt concrete cores are prepared from samples obtained in 2002 from a real underground seal structure which had been installed in 1992 at a depth of 945 m. The salt concrete had been prepared of 18 wt.% blast-furnace cement, 10 wt.% NaCl brine and 72 wt.% salt grit. It has a grain density of about 2200 kg/m^3, a porosity of 6 % and a residual moisture content of 2 %. The cores of rock salt were drilled from the EDZ around the sealing element.

The salt concrete core (diameter 35 mm) is placed accurately fitting in the hollow cylinder (70 mm outer diameter by 100 mm height). In order to fill up potentially remaining voids, the core is coated with salt slurry and then pushed into the hollow salt cylinder. Excess slurry is removed, and the sample is dried in an oven to avoid undefined saturation states.

A photo of a salt concrete core, a hollow cylinder and the completed sample is shown in Fig. 3.1.
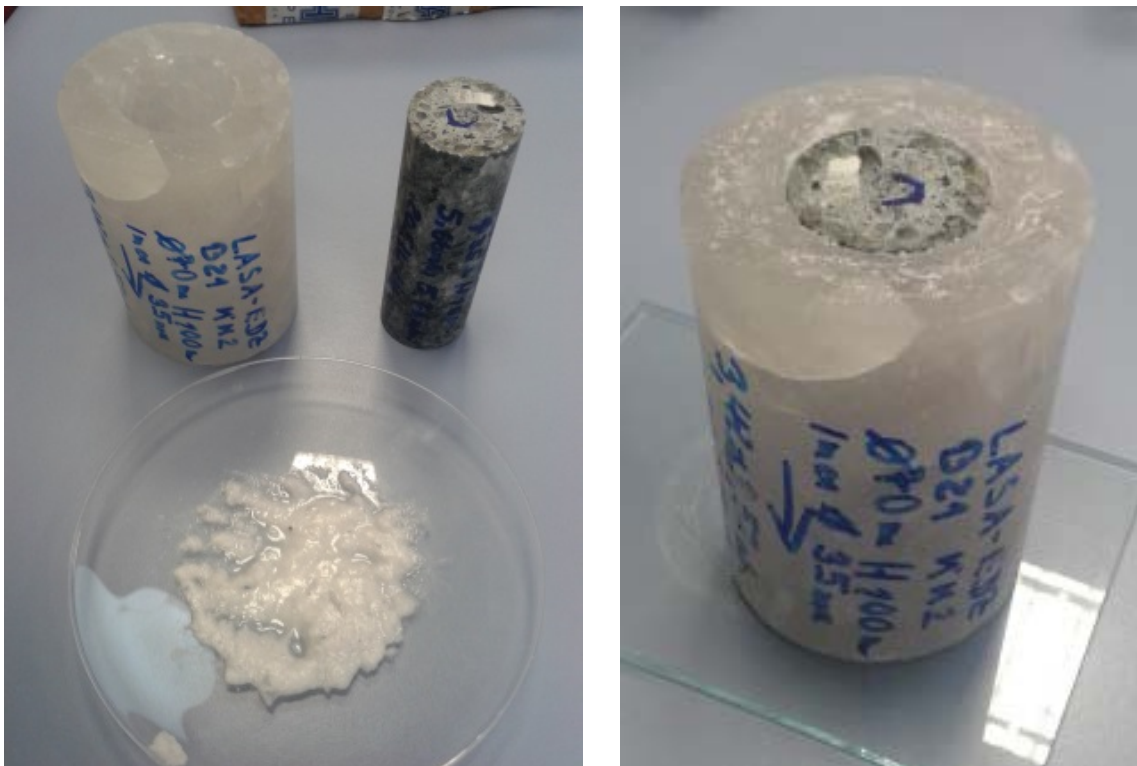

Fig. 3.1   Hollow salt cylinder, salt concrete core and salt slurry (left); complete combined sample (right)

The samples are coated with rubber jackets and placed in isostatic cells equipped with hydraulic lines to allow for axial flow-through of gas or liquid and determination of the system permeability as shown in Fig. 3.2.

A photo of a coated sample and the cell arrangement is shown in Fig. 3.3.
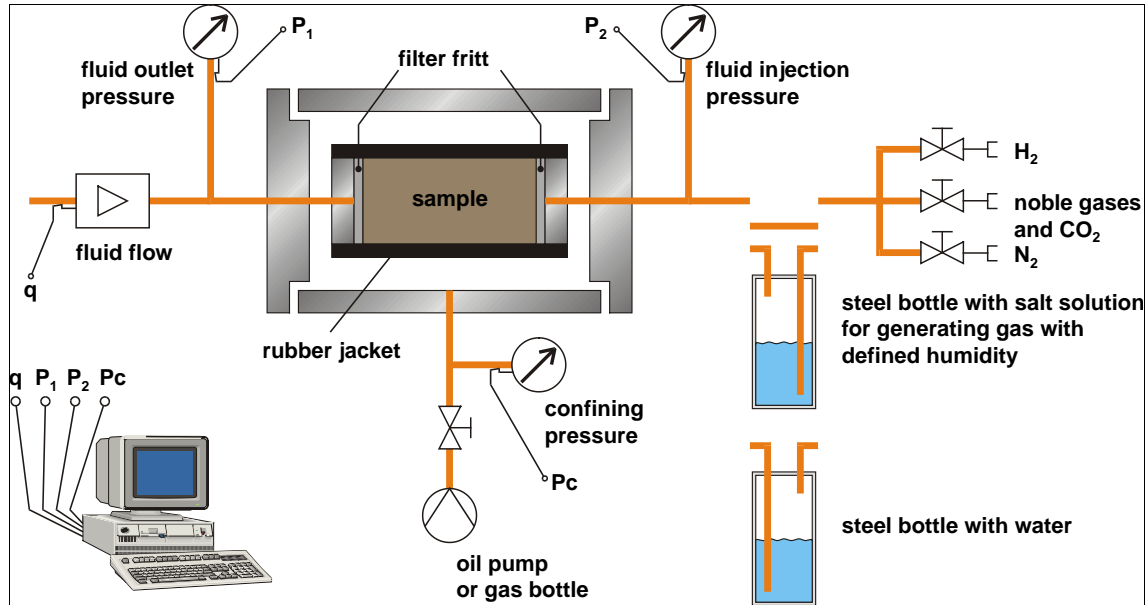

Fig. 3.2   Principal sketch of the modified Hassler cell for determining gas and water permeability

Fig. 3.3   Coated test sample (left); test equipment (right)

The cores were covered with a rubber jacket on the surface and two pistons on both ends. These pistons had a lead through for the fluids (gas or brine) which were used for the permeability measurements. In order to inject and withdraw the fluids homogeneously filter frits of stainless steel were placed at both ends between the pistons and the sample. The confining pressure on the sample was

produced by an oil pump or by nitrogen from a gas bottle. This pressure could vary between 0.1 and 15 MPa.

At a special valve panel, the pressure of the test gas (nitrogen) was reduced from the pressure inside the gas tank (up to 20 MPa) to the injection pressure between 0.1 and 0.7 MPa. The injection pressure had to be less than 80 % of the confining pressure in order to avoid gas flow along the surface between the sample and the rubber jacket.

For flooding the pore volume of the sample with brine and for brine permeability measurements this steel bottle could be filled with brine. The injection pressure was then generated by nitrogen connected to the bottle. The flow rate through the sample, the gas injection pressure, the gas outlet pressure and the confining pressure were recorded on a PC and additionally displayed for visual inspection.

The test procedure is first to perform gas permeability tests of the dry sample while stepwise increasing the compressive load. After unloading of the sample saturated brine is injected and the stepwise loading is repeated, while the permeability of the system to brine is recorded. The evolution of the permeability of the composite sample to gas or to brine is the essential variable characterizing the recovery of the EDZ and the closing of the contact seam between salt concrete core and surrounding rock salt.

A pilot test was performed in order to check whether the sample composition and the measurement technique were suitable. After the test, the sample was dismantled and inspected. The pilot test showed that the test method is adequate to investigate evolution of the overall permeability of dry and brine-containing composite samples as a function of compressive load. It also showed that load changes have to be applied cautiously in order to maintain integrity of the testing arrangement. A detailed description is given in /CZA 15/ and /CZA 16/.

3.2 Experimental results

3.2.1 Advection experiments with individual samples

For the start of detailed testing, two new samples were prepared. In order to increase the bandwidth of results, one sample featured an intact salt concrete core as taken from the in situ seal, while for the other sample a larger salt concrete core was loaded triaxially to the failure point and a smaller core was machined from the damaged core. The rationale of using a damaged salt concrete core as seal element is the fact that shrinkage fractures of a seal during construction cannot be excluded. Both the salt concrete cores and the rock salt cylinders were characterized in terms of permeability to gas before preparing the combined samples. Afterwards, gas and liquid testing in the isostatic cells was started similarly to the pilot test. The results of the load-dependent permeability tests of the individual material samples are summarized in Fig. 3.4.
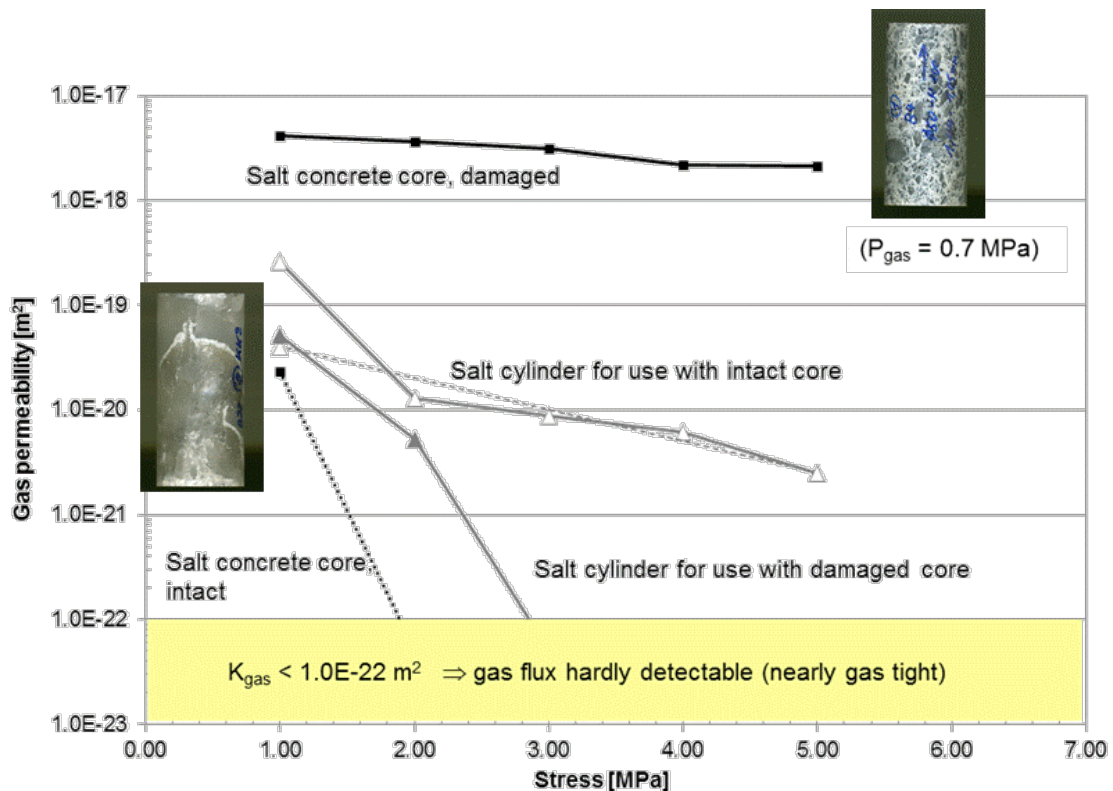

Fig. 3.4 Gas permeability of salt concrete cores and salt cylinders before assembly of combined samples

15

For characterization of the salt concrete cores, these were placed in isostatic cells and the load dependent gas permeability was determined under stepwise loading from 1 to 5 MPa. The permeability of the intact salt concrete core, calculated using Darcy's law, amounted to $2.3 \cdot 10^{-20}\,\text{m}^2$ at 1 MPa isostatic load and fell below $1.0 \cdot 10^{-22}\,\text{m}^2$ already at 2 MPa. This also showed that flow along the jacket interface is not an issue.

For the damaged core, a moderate permeability decrease from $4.1 \cdot 10^{-18}\,\text{m}^2$ at 1 MPa load to $1.6 \cdot 10^{-18}\,\text{m}^2$ at 5 MPa was observed. The salt cylinders were subjected to the same tests before drilling the central holes for reception of the salt concrete cores. They also showed a permeability decrease with load: From $2.6 \cdot 10^{-19}\,\text{m}^2$ to $2.5 \cdot 10^{-21}\,\text{m}^2$ for the cylinder used with the intact salt concrete core and from $5.2 \cdot 10^{-20}\,\text{m}^2$ to below $1.0 \cdot 10^{-22}\,\text{m}^2$ for the cylinder used with the damaged one.

3.2.2 Advection experiments with salt concrete sealing elements and dilated rock salt

After characterization of the salt concrete and salt cores, the central holes were drilled into the salt cylinders and the combined samples were prepared as described earlier. The potential effect of the sub-coring on the salt core gas permeability could not be quantified.

In the first stage of testing the combined samples, the confining load was increased by 1 MPa steps to 5 MPa over two weeks and gas flowed axially through the samples. For the sample with the intact seal element of salt concrete, the gas permeability decreased slightly from $2.5 \cdot 10^{-14}\,\text{m}^2$ to $1.3 \cdot 10^{-14}\,\text{m}^2$. When the sample was unloaded, the gas permeability remained at this value. The permeability measured was close to the upper limit of the testing arrangement. In fact, for the sample with damaged seal element gas permeability remained above the upper measurement limit of $5 \cdot 10^{-14}\,\text{m}^2$.

The gas tests on dry samples showed the high impact of the contact seam – the overall permeability was much higher than the gas permeabilities of the individual

materials. A second result of gas testing was that under dry conditions and moderate confining stress up to 5 MPa, a reconsolidation of the EDZ or a closing of the contact seam is negligible in the short term.

After gas testing, the samples were unloaded, and brine was injected. Then, the samples were again loaded in steps of 1 MPa up to 5 MPa, and the permeability to brine was measured. The measurement results are shown in Fig. 3.5. The time until maximum load was three weeks for the two samples. Both samples showed a significant decrease of permeability to liquid with increased loading.
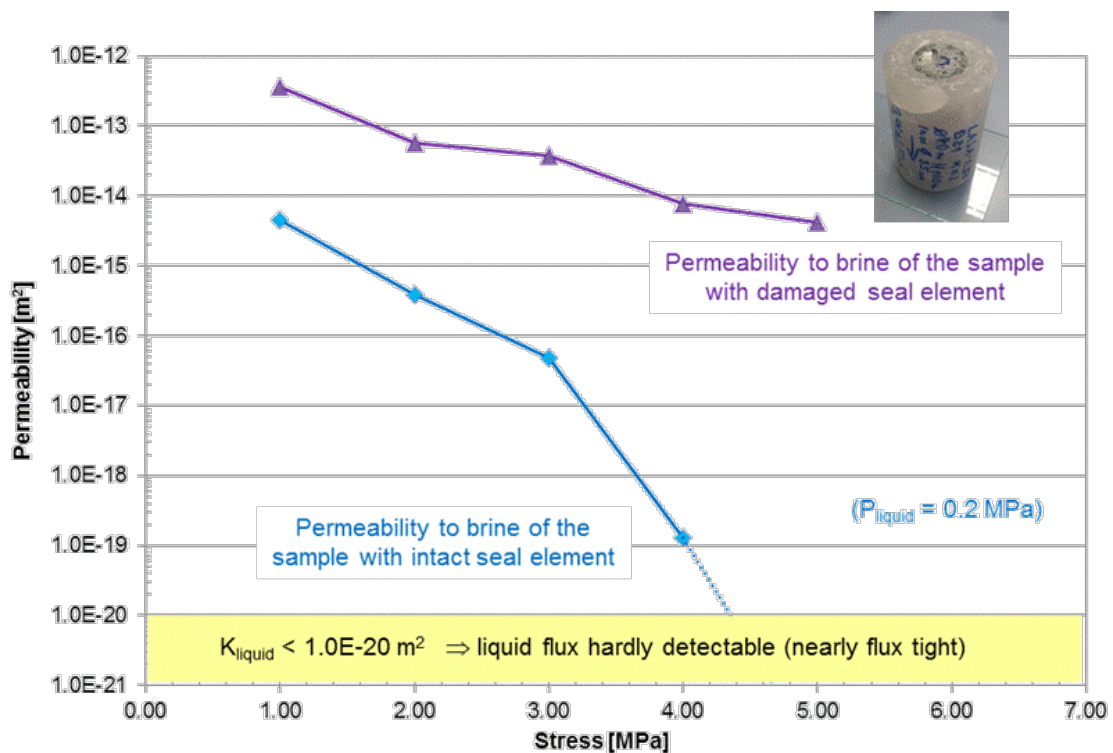

Fig. 3.5   Permeability of combined samples as a function of confining stress

For the sample with the intact seal element, permeability decreased from an initial value of $4.5 \cdot 10^{-15}\,m^2$ to below the detection limit of $1.0 \cdot 10^{-20}\,m^2$ at a load of 5 MPa. Obviously, the salt surrounding the seal element became soft enough to enable very effective sealing of the contact seal and the EDZ in short time. The sample behaved significantly differently from the dry case, where only a slight gas permeability reduction was observed. Afterwards, the sample was gradually unloaded again. Permeability remained below the detection limit, showing that

17

irreversible compaction had occurred. It is envisaged to dismantle the sample and confirm the reconsolidation and associated reduction of pathways by microscopic inspection.

As expected, the sample with the damaged seal element started at a higher permeability of $3.6 \cdot 10^{-13}\,m^2$ (please note that the measurement limits for permeability measurement with liquid are different from those for gas tests). With increasing confining stress the permeability decreased by two orders of magnitude, but it remained much higher than for the sample with the intact seal element.

While a compressive load of 5 MPa was sufficient to effectively seal the contact zone and the EDZ in the presence of brine in the experiment with the intact seal element, the same cannot be postulated for the experiment with the damaged seal element. Obviously, reconsolidation of the damaged seal element has not been achieved. The permeability value measured at 5 MPa confining stress, however, seems too high to attribute it to the flow through the seal element alone, as the gas permeability of the damaged salt concrete ranged between $1 \cdot 10^{-18}\,m^2$ and $1 \cdot 10^{-17}\,m^2$ (see Fig. 3.4).

This sample was not unloaded. The confining stress was increased in steps up to 10 MPa and the measurement of permeability to brine continues. Fig. 3.6 shows the permeability to brine as a function of time.
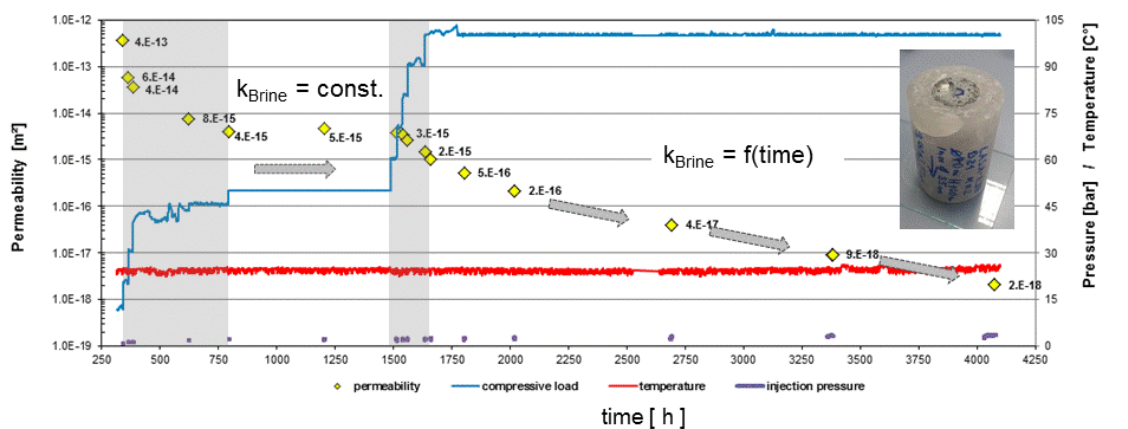

Fig. 3.6   Permeability to brine of the sample with damaged seal element as a function of time

Obviously, the permeability value decreased not only with increasing confining pressure (light grey phase). The measurements showed a decrease of more than two orders of magnitude from $1 \cdot 10^{-15}$ m^2 down to $1 \cdot 10^{-18}$ m^2 within the next 100 days (2400 hours). It is expected, that the permeability value will tend towards the detection limit without further increase of the confining pressure.

The experimental set-up was applied to eight combined samples, varying the confining stress with time. In general, this procedure resulted in a decrease of permeability in all combined samples, see Fig. 3.7. For detailed description of the testing procedure and the discussion in depth the authors refer to /JAN 18b/.
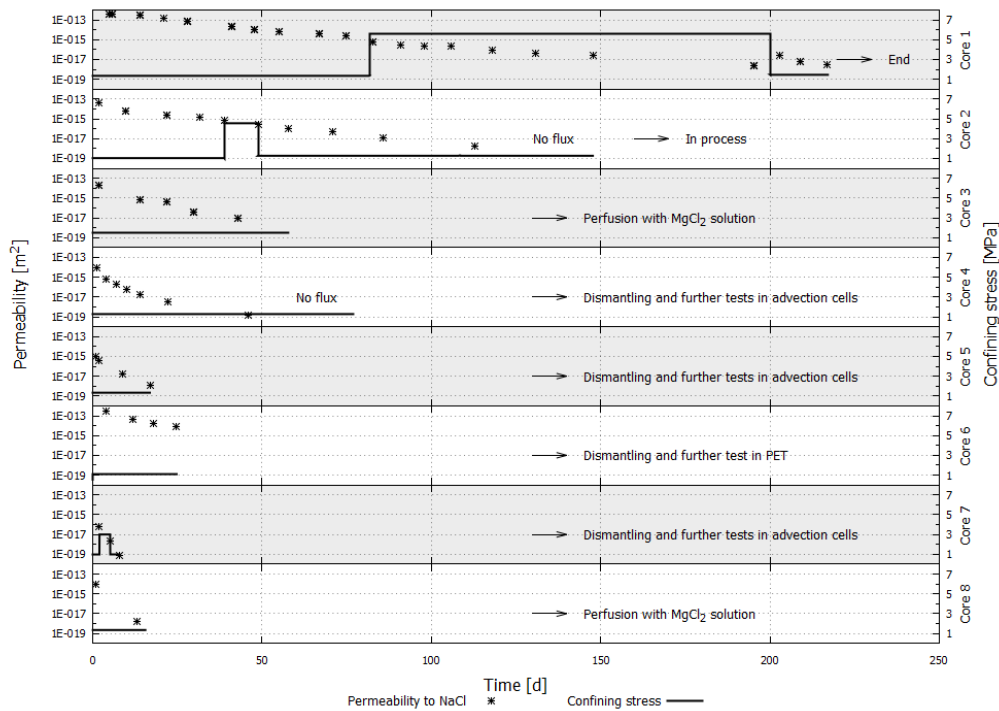

Fig. 3.7   Permeability measurements of combined samples with NaCl-solution at injection pressure of 0.1 MPa and varying confining stress /JAN 18b/

It can be summarized that reduction of permeability needed more time in samples with a higher initial permeability. During fabrication of the combined samples, it was generally observed that the samples with a concrete plug fitting smoothly

into the hollow cylinder had a higher initial permeability than those exhibiting friction while inserting the plug.

Hence, the accuracy of preparation of the salt concrete core and the rock salt cylinder in the turning machine influenced significantly the initial permeability of the combined samples. This finding supports the assumption that the contact seam is the primary pathway for solutions.

The influence of the confining stress on the evolution of hydraulic conductivity of the contact seam did not follow a consistent pattern: core 1 showed that a reduction of the confining stress resulted in an increase of permeability while in core 2 no dependence was observed. The impact of the increased confining stress in core 7 could not be finally evaluated: therefore, further investigations on combined samples with low initial permeability are needed. Probably, the increased confining stress accelerated the decrease of permeability.

However, experiments aimed primarily at the investigation of the hydro-mechanical behaviour of the contact seam and at developing a method to produce suitable combined samples for this purpose.

3.2.3   Advection experiments with consideration of pore pressure evolution

As stated in chapter 1 there is also a need for testing samples at scenario iii, when the sealing system is nearly fully saturated, and as a result to viscous deformation processes, positive pore pressures can evolve with a certain influence on the sample permeability. Therefore, a pilot test with a pre-damaged salt concrete sample was performed in order to check whether the measurement technique for fluid back pressures at inlet and outlet valves was suitable.

The next Fig. 3.8 shows, for a pre-damaged salt concrete sample, the evolution of the fluid pressure at inflow and outflow valves used for measurement of brine permeability at constant minimum oil pressure. During the first 700 hours the

sample was stressed by a circumferential oil pressure of 50 bars. Additionally, fluid permeability measurements were conducted from time to time. The derived permeability values showed a decrease with time from $4 \cdot 10^{-16}$ m^2 down to $2 \cdot 10^{-18}$ m^2. A regression line shows the general trend.

At approx. 800 days the fluid pressure inside the sample is set to 10 bars and kept constant for 100 days. In figure 6 the dark blue resp. light blue lines highlight the measured fluid back pressure at the inlet and outlet valves. At 910 days the permeability measurement test was performed. According to Darcy, the outlet fluid pressure was decreased to atmospheric pressure and the measurement starts. After the permeability measurement is finished the outlet valve was closed and the fluid pressure starts to increase again. From the measurement data a permeability value of $1 \cdot 10^{-18}$ m^2 could be derived.

At 1100 hours the oil pressure was increased to 100 bars. As a result, the induced compaction of the sample the fluid back pressures suddenly exceeded the pressure sensor detection limit of 12 bars. Then the outlet valve was shortly opened and the values decreased below the sensor limit. Within the next 150 hours both fluid back pressures increased again, maybe due to viscous deformation processes of the sample pore space.

At 1260 hours the sensor limit was reached again and the oil pressure was decreased to the reference value of 10 bars for another fluid permeability test. At a testing time of 1340 hours, a fluid permeability value of $1 \cdot 10^{-18}$ m^2 could be derived, Fig. 3.9.

The test was continued as a drained one with open valves, so that no pore pressure could evolve when the circumferential oil pressure was exceeded again for 500 hours. Finally, no fluid flux through the sample could be detected at the reference level of 10 bars.
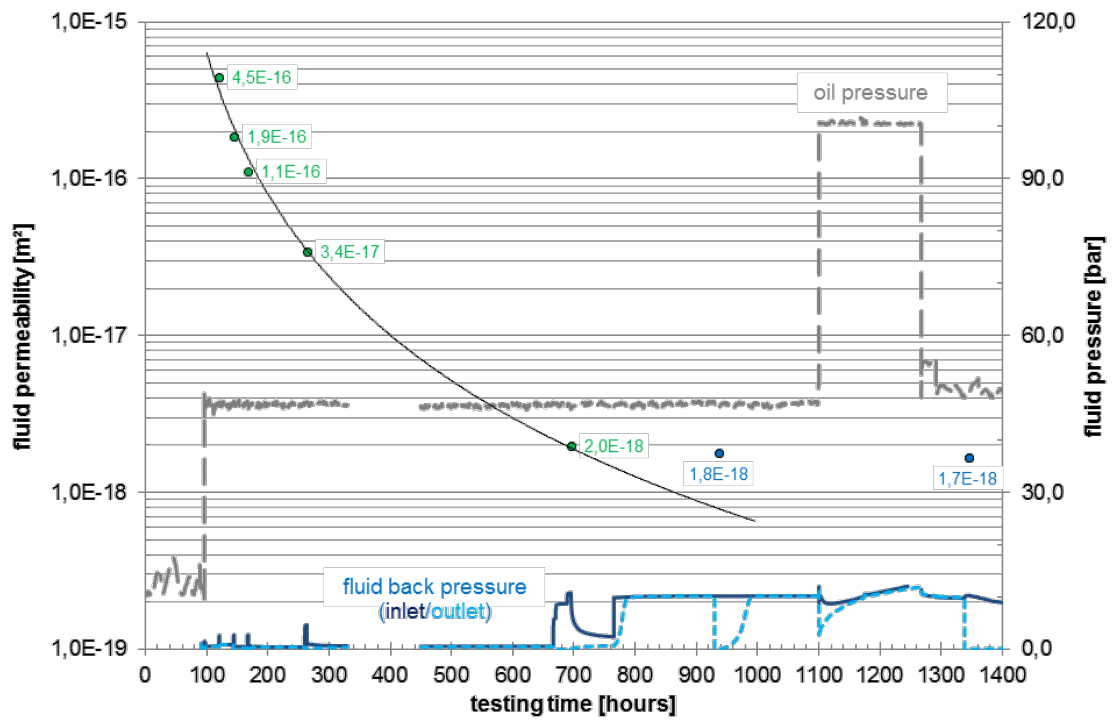
Fig. 3.8 Permeability measurement on a pre-damaged salt concrete sample
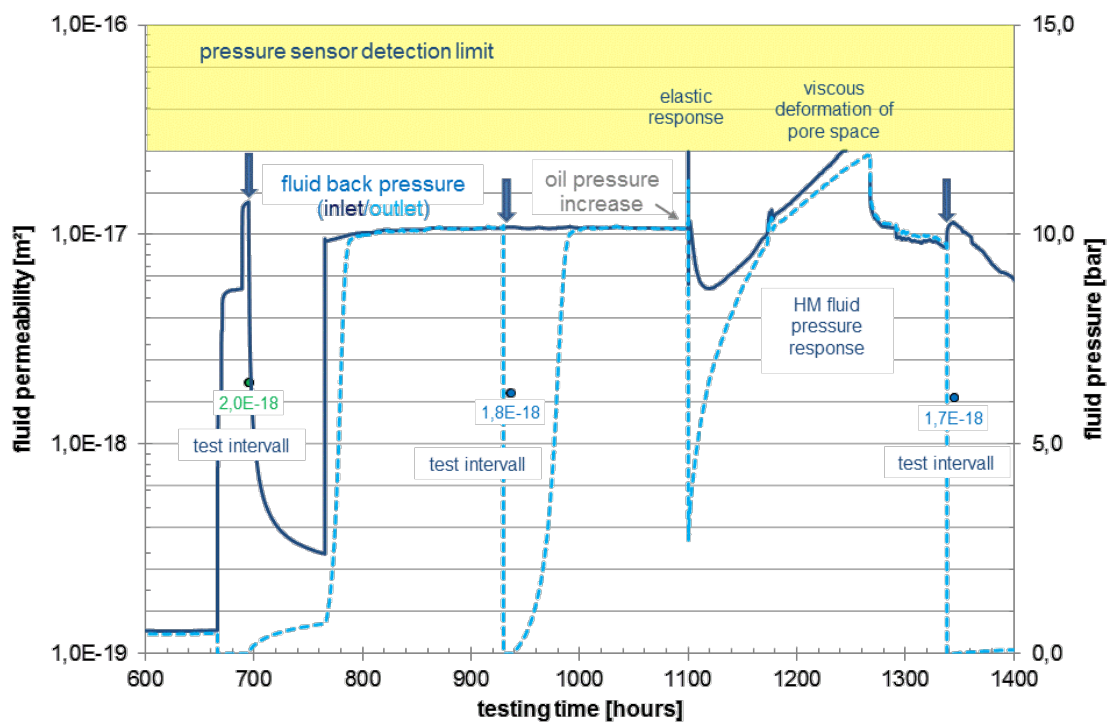

Fig. 3.9 Permeability measurement on a pre-damaged salt concrete sample, detailed view from 600 to 1400 days

3.3　　　Interpretation and discussion

The program aims at providing experimental data needed for the theoretical analysis of the long-term sealing capacity of the seal system, including the closing of the contact seam and the recovery of the excavation damaged zone (EDZ) under load and dry or wet conditions. The interaction with sealing materials is simulated in laboratory tests by using hollow cylinders of salt equipped with a central concrete seal in isostatic cells. The experimental set-up was applied to eight combined samples, varying the confining stress with time. In general, this procedure resulted in a decrease of permeability in all combined samples. It can be summarized that reduction of permeability needed more time in samples with a higher initial permeability. Hence, the accuracy of preparation of the salt concrete core and the rock salt cylinder in the turning machine influenced significantly the initial permeability of the combined samples. This finding supports the assumption that the contact seam is the primary pathway for solutions.

The influence of the confining stress on the evolution of hydraulic conductivity of the contact seam did not follow a consistent pattern. Therefore, further investigations on combined samples with low initial permeability are needed. Probably, the increased confining stress accelerated the decrease of permeability.

Furthermore, a pilot test with a pre-damaged salt concrete sample was performed in order to check whether the measurement technique for fluid back pressures at inlet and outlet valves was suitable. For that purpose, that the sealing system is nearly fully saturated, and as a result to viscous deformation processes, positive pore pressures can evolve with a certain influence on the sample permeability. The results of the pilot test clearly showed a decreasing fluid permeability with time. The process of decreasing permeability stops when positive pore pressures evolve.

However, these results showed only a first characteristic trend that should be confirmed by systematic investigations on combined samples.

4 Basics for numerical modelling

4.1 Scope of calculation work

Within the former THERESA project existing constitutive models for the thermal-hydraulic-mechanical (THM) behaviour of the excavation damaged zone (EDZ) in rock salt, particularly its long-term behaviour and its self-sealing ability under the conditions that will occur in and near repositories were reviewed. Based on the data sets previously compiled, the constitutive models for the EDZ behaviour were calibrated as far as possible and/or improved. Test calculations were carried out and the numerical results were compared with experimental results to demonstrate the suitability of the models. Supporting laboratory tests were additionally performed at GRS' geotechnical laboratory to provide more reliable experimental data for the validation of the models. International modelling teams performed predictions of the laboratory benchmark tests for checking the capabilities of the models to describe the relevant processes, such as EDZ generation and sealing/healing, using the computer codes involved.

The focus of the modelling study in LASA-EDZ was placed on

1. calibration of existing constitutive models of rock salt for coupled THM processes using relevant data, either already available or concurrently produced,

2. laboratory benchmark tests for the validation of the calibrated constitutive models and computer codes, and

3. application of validated models and codes for the simulation of contact zone evolution, taking into account requirements the loading history of the dilated salt rock.

Therefore, the followings sections give an overview of existing constitutive models available in CODE_BRIGHT so far, resume the former calibration work related to the EC-Project THERESA and discuss different approximations to simulate the contact zone evolution.

4.2 Physical Modelling

The following section contains a description of the constitutive model for saline materials that is implemented in CODE_BRIGHT and a description of the work done for its application to EDZ problems. The constitutive model has been described in Olivella and Gens /OLI 02/ and the main purpose was to understand and simulate crushed salt deformations both under dry and wet conditions, for general stress states. In this sense the model is macroscopic and can be applied for any stress state. Although the model was calibrated in a comprehensive way for crushed salt compression it is also able to produce dilatant deformations under certain deviatoric stress states. In what follows the main mechanisms of deformation included are described and the corresponding equations given. The model has three contributions corresponding to FADT creep, dislocation creep and viscoplasticity.

4.2.1 Fluid Assisted Diffusional Transfer (FADT)

As shown in Fig. 4.1, FADT is a deformation mechanism assisted by brine (small amounts) and is based on dissolution at contacts (induced by chemical potential increases due to compression) plus molecular diffusion and final precipitation in pores. This means from contact to pore migration of salt; however, it can also take place from contact to contact in the case that the material is subjected to deviatoric stress states.
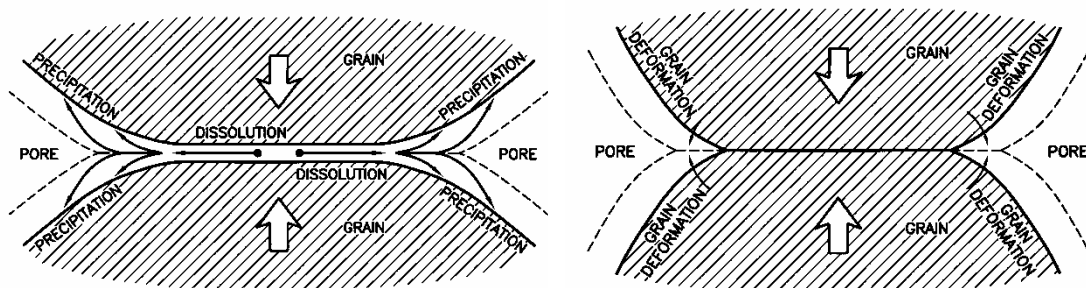

Fig. 4.1   Representation of FADT (dissolution, diffusion and precipitation of salt) and DC creep (particle deformation through crystal dislocation processes)

Migration of salt from contact to pore is associated with a volumetric deformation while migration from contact to contact produces deviatoric deformations. In this sense, as porosity decreases the deviatoric part remains active while the volumetric deformation also disappears progressively.

The final equations for FADT mechanism express strain rate as a function of several variables. These are: stresses, void ratio, grain size, temperature and medium properties. The linear dependence on stresses allows postulating a viscoelastic form.

$$\frac{d\varepsilon_{ij}^{FADT}}{dt} = \frac{1}{2\eta_{FADT}^{d}}(\sigma'_{ij} - p'\delta_{ij}) + \frac{1}{3\eta_{FADT}^{v}}p'\delta_{ij} \tag{4.1}$$

where σ'_{ij} is the effective stress tensor (defined as $\sigma'_{ij} = \sigma'_{ij} - \delta_{ij}P_f$), P_f is fluid pressure, (gas if unsaturated and liquid if saturated), p' is the mean effective stress ($p' = (\sigma'_{11} + \sigma'_{22} + \sigma'_{33})/3$), δ_{ij} is the Kronecker delta, and the volumetric and deviatoric viscosities are defined as:

$$\frac{1}{\eta_{FADT}^{v}} = \frac{16B(T)\sqrt{S_l}}{d_0^3}g_{FADT}^{v}(e) = C(T, S_l, d_o)g_{FADT}^{v}(e)$$

$$\frac{1}{2\eta_{FADT}^{d}} = \frac{16B(T)\sqrt{S_l}}{d_0^3}g_{FADT}^{d}(e) = C(T, S_l, d_o)g_{FADT}^{d}(e) \tag{4.2}$$

$$g_{FADT}^{v}(e) = \frac{3g^2 e^{3/2}}{(1+e)} \quad g_{FADT}^{d}(e) = \frac{g^2}{(1+e)} \quad g = \frac{1}{(1-f)^2} \quad f = \sqrt{\frac{2e}{3(1-e^{3/2})(1+e)}}$$

$$\tag{4.3}$$

The function $C(T, S_l, d_o)$ includes the information related essentially to grain size, brine content and temperature. The functions g^v_{FADT} and g^d_{FADT}, g and f are geometry-dependent. In principle, change to other grain shapes would modify these functions, while the other dependences would remain unchanged. From experimental data the model parameters determined by Olivella and Gens /OLI 02/ are:

$$B(T) = \frac{6 \times 10^{-13}}{RT} \exp\left(\frac{-24530}{RT}\right) \text{s}^{-1}\text{MPa}^{-1}\text{m}^3$$

Obviously, this part of the model should not be included if the medium is considered dry.

This, however, becomes in a natural way as degree of saturation is equal to zero. In such case, both viscosities tend to infinity and this part of the model vanishes.

4.2.2   Dislocation Creep

Dislocation creep is an intracrystalline deformation mechanism (Fig. 4.1). Both, the rock grains and the crushed salt grains, deform when subjected to deviatoric stress states. The deviatoric deformation of grains produces porosity changes and thus volumetric creep deformations of the material which are only possible if there is some porosity available. The following general form, based on viscoplasticity theories for geological materials, was proposed:

$$\frac{d\varepsilon_{ij}^{DC}}{dt} = \frac{1}{\eta} \Phi(F) \frac{\partial G}{\partial \sigma_{ij}'} \tag{4.4}$$

This is a viscoplastic equation with a flow rule but without a yield condition, so it is active for any stress level. In this equation it has been included: a viscosity parameter, a flow rule (G), a stress function (F) and a scalar function (Φ). In Equation (4.4) G and F should be taken as functions of stress invariants. The following form was proposed:

$$F = G = \sqrt{q^2 + \left(\frac{p}{\alpha_p}\right)^2} \qquad \Phi(F) = F^n \tag{4.5}$$

where n is the power of the rock creep law and α_p is a material parameter. Fig. 4.2 shows the shape of the flow rule in the (p', q) plane depending on F and α_p values.

Since $\Phi(F)$ is always positive, no threshold is considered in this law. This is consistent because saline rocks develop viscous deformations under any stress level. In order to exploit the theoretically derived equations this generalization of the model is complemented with definitions for η and α_p:

$$\eta = \eta_{DC}^{d} \qquad\qquad \alpha_p = \left(\frac{\eta_{DC}^{v}}{\eta_{DC}^{d}} \right)^{\frac{1}{n+1}} \qquad\qquad (4.6)$$

When void ratio vanishes α_p tends to infinity and the mathematical expression of G (eq. 4.5) reduces to the von Mises case. In this way the creep law for rock salt with von Mises flow rule is recovered. Therefore α_p can be seen as a hardening parameter for volumetric creep behaviour. With the flow rule adopted, the model does not allow any dilatancy behaviour.
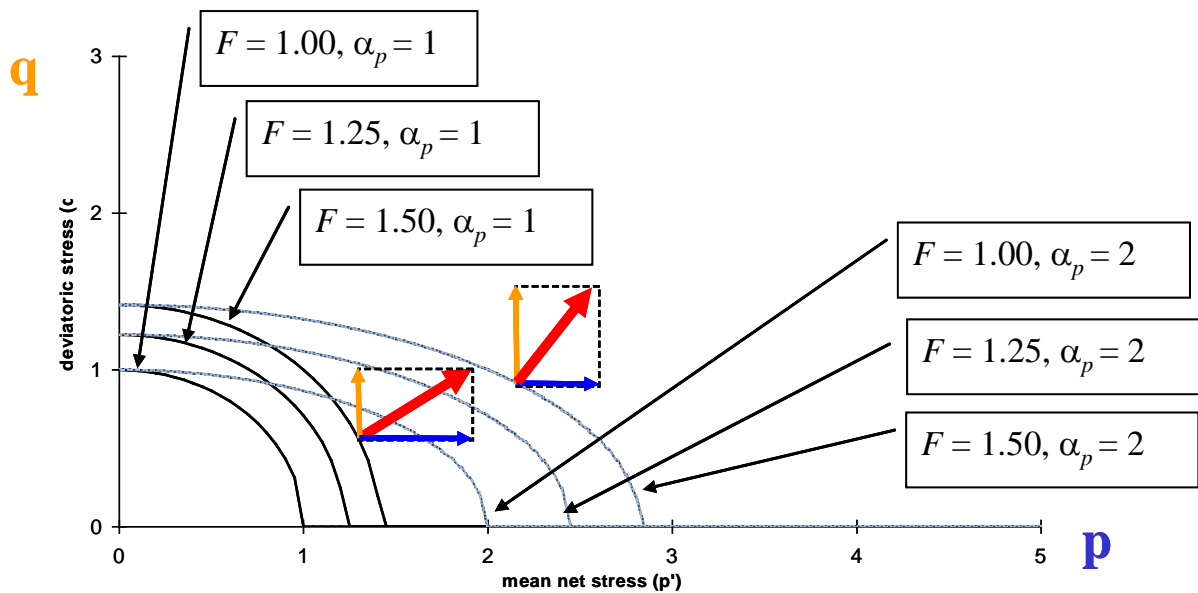
Fig. 4.2   Stress function and flow rule $F = G$ used for the viscoplastic generalization of the creep model (DC mechanism)

(Note that depending on the mean stress and deviatoric stress levels, deformations are different)

Additional relationships for the creep model are the viscosities and the void ratio functions:

$$\frac{1}{\eta_{DC}^{v}} = A(T)g_{DC}^{v}(e) \qquad\qquad \frac{1}{\eta_{DC}^{d}} = A(T)g_{DC}^{d}(e) \qquad\qquad (4.7)$$

$$g_{DC}^{v}(e) = 3(g-1)^{n}f \qquad\qquad g_{DC}^{d}(e) = \left(\sqrt{\frac{1+g+g^{2}}{3}}\right)^{n-1}\left(\frac{2g+1}{3}\right)f + \frac{1}{\sqrt{g}} \qquad (4.8)$$

$$g = \frac{1}{(1-f)^{2}} \qquad f = \sqrt{\frac{2e}{3(1-e^{3/2})(1+e)}}$$

The parameters determined in /OLI 02/ for the dislocation creep component are:

$$n = 5, \quad Q_{DC} = 54000 \text{ J/mol}, \quad A_{DC} = 5.8 \times 10^{-6} \text{ 1/s}$$

This creep part of the model is based on dislocation theory or, in other words, on power law for rock salt. This is a purely creep model. The initial void ratio gives the initial creep compressibility of the material.
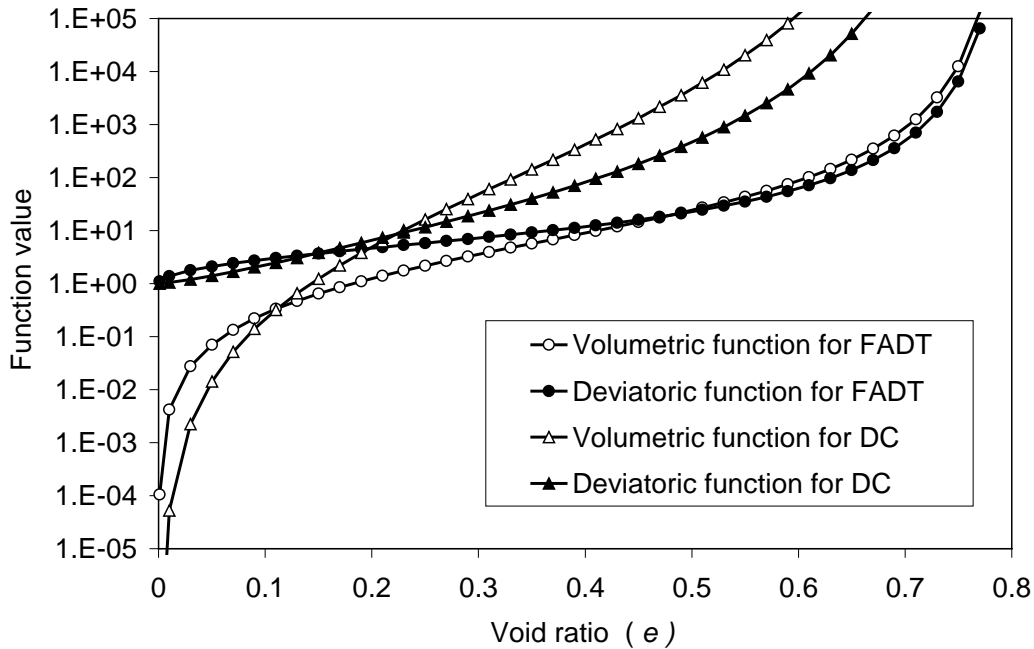
Fig. 4.3 Auxiliary functions g^{v}_{FADT}, g^{d}_{FADT}, g^{v}_{DC} and g^{d}_{DC} that appear in the viscosities

The two creep components to the model (FADT and DC) share the same geometry for equation development and the internal variable void ratio (e). As void ratio (or porosity) changes, the FADT and the DC functions are modified. Fig. 4.3 shows that hardening takes place when void ratio decreases but variations depend on the range.

4.2.3   Additional viscoplastic term enabling dilatancy

The constitutive model of Olivella and Gens /OLI 02/ described above was developed for crushed salt deformation. When the crushed salt becomes dense it resembles the rock salt and following this idea it seems that a constitutive model may be applicable to both crushed salt and rock salt. However, the model for crushed salt is essentially a model for compaction under isotropic and deviatoric stress states. This model is in fact appropriate for the simulation of deformations under stress states falling in regions (2) and (3) in Fig. 4.4. This implies relatively low deviatoric / mean stress ratio (low q/p). In fact, the model was only able to calculate volumetric deformations of compression in addition to deviatoric, but not in dilatant conditions.
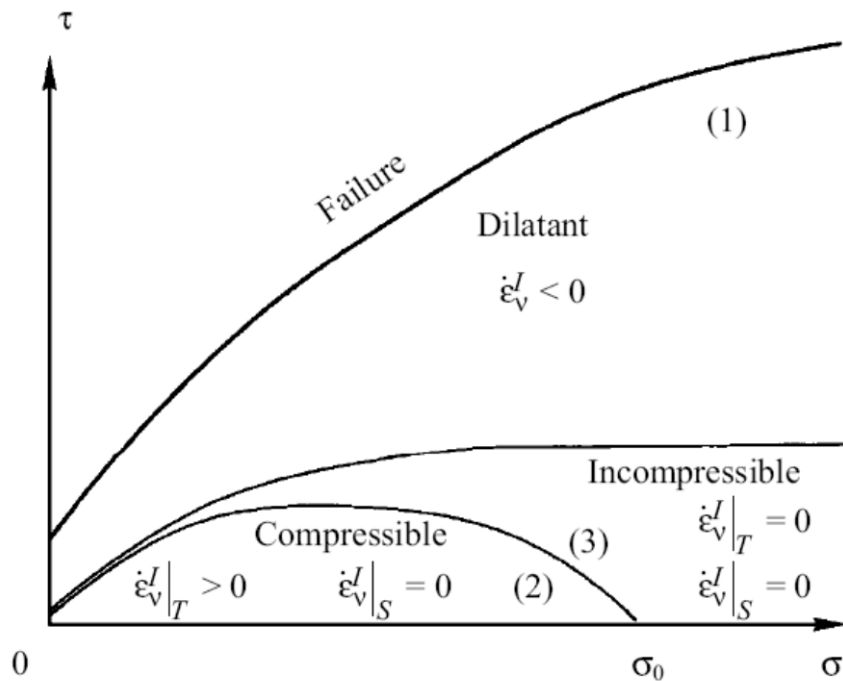
Fig. 4.4   Different deformation types depending on the stress state /CRI 02/

31

In order to simulate the behaviour of rock salt under dilatant conditions, i. e. for stress states falling in the region (1) in Fig. 4.4, it is necessary to consider an additional term to the model. In this way, the overall model equations have the form:

$$\frac{d\varepsilon_{ij}}{dt} = \left(\frac{d\varepsilon_{ij}}{dt}\right)^{elastic} + \left(\frac{d\varepsilon_{ij}}{dt}\right)^{FADT} + \left(\frac{d\varepsilon_{ij}}{dt}\right)^{DC} + \left(\frac{d\varepsilon_{ij}}{dt}\right)^{VP} \tag{4.9}$$

$$\frac{d\varepsilon_{ij}}{dt} = D^{-1}\frac{d\sigma'_{ij}}{dt} + \frac{1}{2\eta^{d}_{FADT}}\left(\sigma'_{ij} - p'\delta_{ij}\right) + \frac{1}{3\eta^{v}_{FADT}}p'\delta_{ij} +$$
$$+ \frac{1}{\eta^{d}_{DC}}\Phi^{DC}\left(F^{DC}\right)\frac{\partial F^{DC}}{\partial\sigma'_{ij}} + \frac{1}{\eta^{d}_{VP}} < \Phi\left(F^{VP}\right) > \frac{\partial G^{VP}}{\partial\sigma'_{ij}} \tag{4.10}$$

The additional viscoplastic term (VP) is useful for rock salt and for crushed salt. The decomposition of this term has to be chosen depending on the stress state. In Olivella and Gens /OLI 02/ the viscoplastic part was included to model compaction of crushed salt by grain crushing and reorganization. However, in the case of rock salt under dilatant conditions, the viscoplastic part of the model may require a different shape.

In rock salt creep deformations hardening and dilatancy occur. These are observed when triaxial tests are performed under stress states falling in the region (1) of Fig. 4.4. These deformations are represented by the viscoplastic component to the model which is combined with the creep part. This viscoplastic part is quite powerful because several yield functions and flow rules can be used (associated or non-associated) and complemented by hardening and softening laws both for the size and for the shape of these yield and flow rules.

The basic viscoplastic equation is:

$$\frac{d\varepsilon^{VP}_{ij}}{dt} = \frac{1}{\eta^{d}_{VP}} < \Phi(F^{VP}) > \frac{\partial G^{VP}}{\partial\sigma'_{ij}} \tag{4.11}$$

The brackets <Φ> indicate that this mechanism is only active when Φ > 0. The yield function (*F*) and the viscoplastic flow rule (*G*) have been adopted to model the response of rock salt under triaxial conditions in the following way:

$$F = a_1 q - bp$$
$$G = a_1 q - \alpha bp \qquad (4.12)$$
$$\Phi(F) = F^m \text{ for } F \geq 0; \quad \Phi(F) = 0 \text{ for } F < 0$$

$$b = a_3 + a_2 (W_d)^{0.25} - a_4 \langle W_d - W_{d0} \rangle^{0.25}$$
$$\alpha = a_5 + a_6 \left(W_d + \langle W_d - W_{d0} \rangle^2 \right) \qquad (4.13)$$
$$dW_d = q d\varepsilon_d$$

This is a relatively simple non-associated model with hardening/softening based on the irreversible work hardening. Because the function *F* is positive for a certain stress states, the viscoplastic contribution is only active in that region.

4.3 Former calibration work related to the EC-Project THERESA

The aim of THERESA project was to develop a scientific method for evaluating the capabilities of mathematical models and computer codes used in Performance Assessment (PA) - using process level models - or Total System Performance Assessment (TSPA) - mostly using simplified PA models. The project was applied to the design, construction, operation, performance and safety assessment, and post-closure monitoring of geological nuclear waste repositories, based on the scientific principles governing coupled thermo-hydro-mechanical and chemical (THMC) processes in geological systems and geo-materials. The project work concentrated on the most essential issues for PA identified in the Issue Evaluation Tables (IET), with a focus on rock salt, buffer materials, and the buffer-rock interface. Details on the overall contents of the project can be found in the description of work /DOW 06/, annex I to the project contract.

Two different types of host rock were considered within this project, rock salt, as it is the mostly considered host rock in Germany covered in Work Package 3 (WP3), and hard rock (WP4). With respect to the German point of view, the German participants in THERESA project are cooperated in WP3. WP3 of the project addressed the evaluation and improvement of numerical modelling capabilities for assessing the performance and safety of nuclear waste repositories in rock salt, with particular emphasis on the long-term evolution of the excavation damaged zone (EDZ), which is one of the most important issues identified in the IET for rock salt. The work related to rock salt disposal consisted of the following components:

The existing constitutive models for the thermal-hydraulic-mechanical (THM) behaviour of the excavation damaged zone (EDZ) in rock salt, particularly its long-term behaviour and its self-sealing ability under the conditions that will occur in and near repositories were reviewed, and all relevant results obtained within the scope of earlier projects (e.g., NF-PRO, national programmes) were compiled, evaluated, and discussed with regard to their usability for calibrating the different models /WIE 07/.

Based on the data sets previously compiled, the constitutive models for the EDZ behaviour were calibrated as far as possible and/or improved. Test calculations were carried out and the numerical results were compared with experimental results to demonstrate the suitability of the models /WIE 08/.

Supporting laboratory tests were performed at GRS' geotechnical laboratory to provide more reliable experimental data for the validation of the models calibrated in work packages WP3.1 and WP3.2. The definition of the test case, the laboratory BMT of WP3, was discussed and agreed upon the WP3 members, and the tests were then conducted. The technical definition of the BMT and its experimental results are described in /ZHA 09/.

The modelling teams performed predictions of the laboratory benchmark tests for checking the capabilities of the models to describe the relevant processes, such as EDZ generation and sealing/healing, using the computer codes involved /WIE 09/.
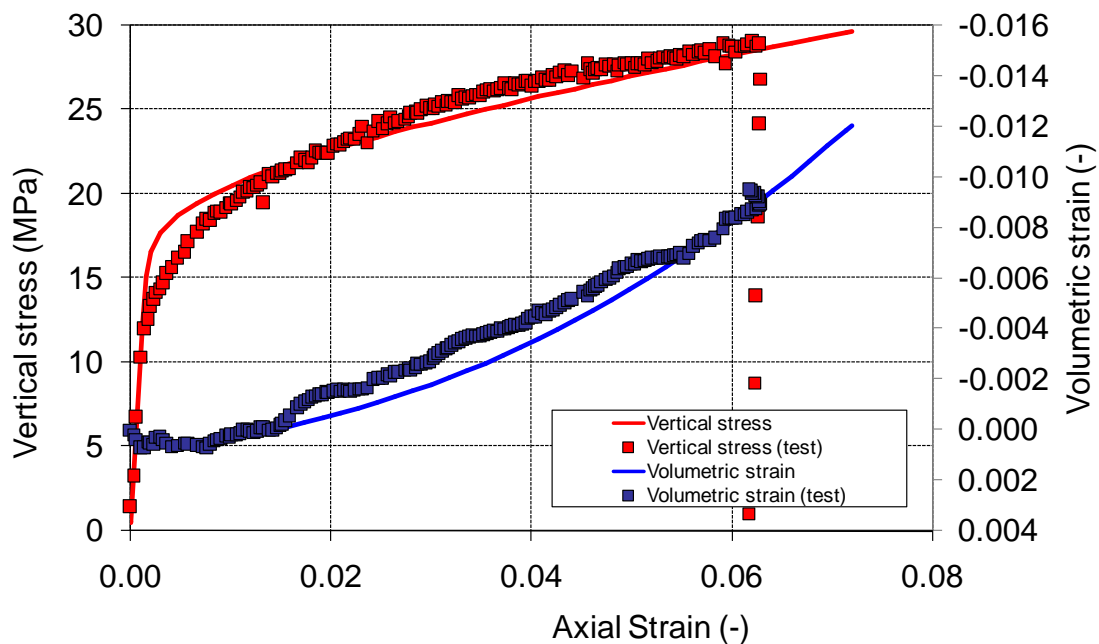
Fig. 4.5   Simulation of a triaxial test at confining stress of 1 MPa, strain rate 10^{-7} s^{-1}, T=30 °C, pore pressure of 0.5 MPa on a sample from 800 m level at Asse

The first test to be simulated was the triaxial tests that has been performed by GRS at confining stress of 1 MPa, strain rate of 10-7 s-1, T=30 °C, pore pressure of 0.5 MPa on the sample from 800 m level at Asse salt mine. The measurements and the calculated results are represented in Fig. 4.5.

The parameters that have been used for the model calculations shown in Fig. 4.5 are the following (Tab. 4.1):

Tab. 4.1   Parameters for simulation of the test sample

Elastic	E = 10000 MPa	$\nu = 0.3$	
Dislocation creep	n = 5	$A = 2 \cdot 10^{-6}$ MPa^{-n}s	Q = 54 kJ/mol
Viscoplastic	m = 8	$A = 2 \cdot 10^{-9}$ MPa^{-n}s	Q = 54 kJ/mol
	$a_1 = 2.5$	$a_2 = 1.8$	$a_3 = 2.5$
	$a_4 = 0.7$	$a_5 = 0.02$	$a_6 = 0.02$
	$W_{d0} = 3.5$		

The test using the hollow cylinder apparatus was performed imposing a complex stress path (Fig. 4.6). The stress path was modified during the test in order to achieve permeability increments. Actually, these were only measured when the inner stress was increased above the outer stress. This happens between 30 and 35 days as can be seen in Fig. 4.6.

The permeability calculations are shown in Fig. 4.7 together with the measured values. The model predictions show some trends which are consistent with measurement such as the starting of permeability increase, the decrease during compression (but at lower rate), further increase of permeability during unloading and decrease of permeability at heating. The values are not fully consistent even though the model has been recalibrated using s = 0.01 m, much higher than in the previous tests. The hollow cylinder conditions (tension) are quite different from the triaxial conditions (shear) to obtain dilatancy, so that may help to explain different spacing of fractures. Actually, a localized fracture in the hollow sample was observed, while in the triaxial tests, the same show failure in a more distributed way.
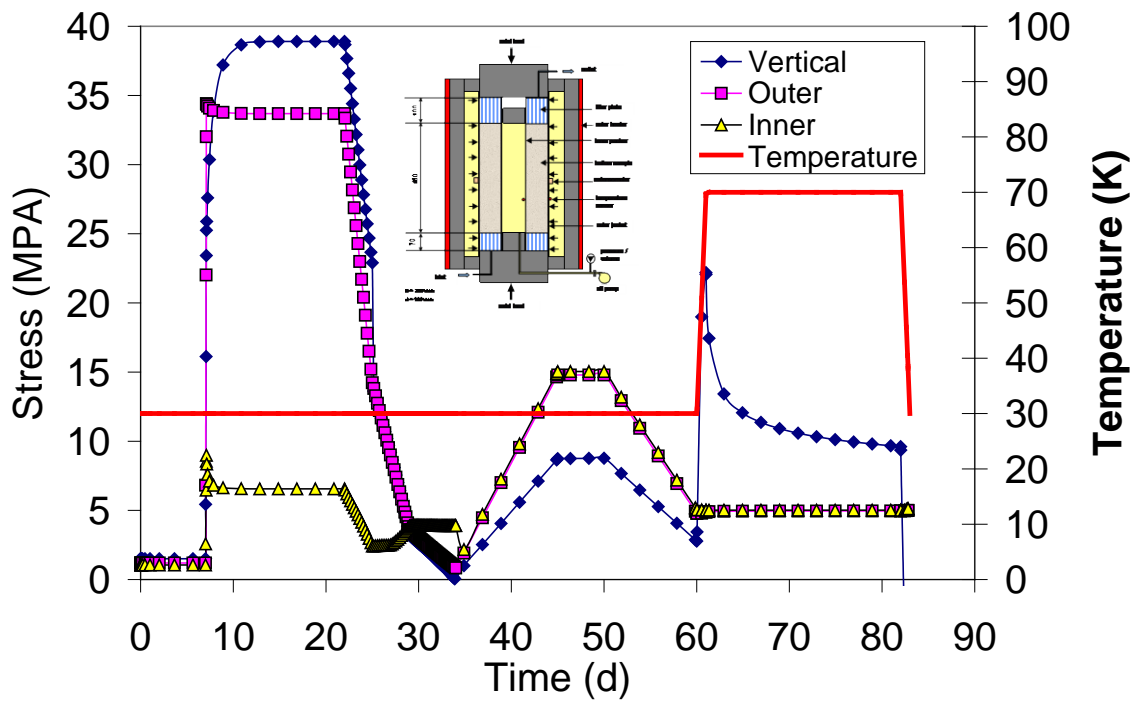
Fig. 4.6 Stress history applied in the hollow test to perform the large scale test
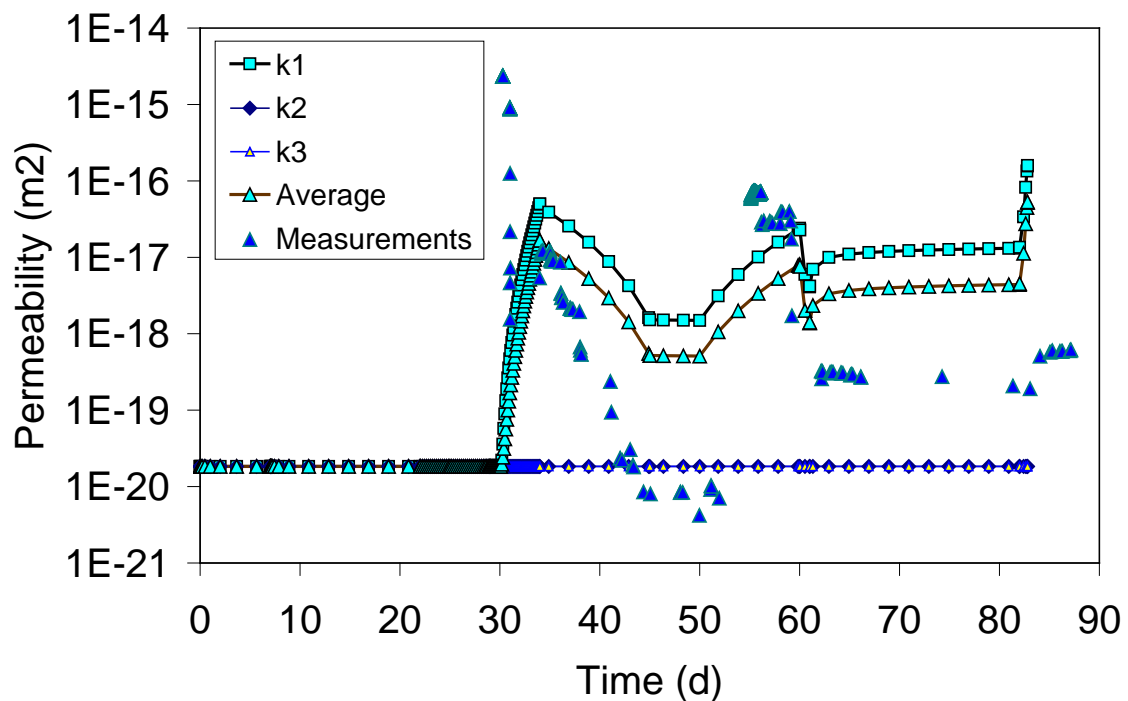
Fig. 4.7 Measured and calculated evolution of permeability (s = 0.01 m)

The predictive capabilities of the constitutive model for saline materials developed originally for crushed salt have been increased by the addition of a contribution to produce dilatancy deformations. This model is empirical and relatively simple. Hardening is produced by a variable that depends on the dissipated shear work.

With the same parameters for the mechanical constitutive models, different tests were simulated. One parameter was modified in order to increase the dilatancy and hence improved the results (the permeability function was recalibrated by changing the spacing of microfractures).

In the case of the hollow cylinder, the parameters were used as well. This gave little dilatancy and hence little change in permeability. In order to get permeability in the order of the measurements, the spacing was increased. This implies fewer fractures in the sample but with higher aperture increase. The fact that triaxial test and hollow test do not give the same function of permeability is not surprising as the deformation mode was very different.

The cubic law applied to apertures derived from deformations is a promising approach because it can be combined with anisotropy; it can be applied to unsaturated conditions by simply using Laplace's Law to calculate the capillary pressure.

However, the determination of the spacing is difficult and assumptions will have to be performed for the predictive application of the model.

4.4 Numerical simulation of the salt concrete sealing elements and dilated rock salt

The modeling task was to simulate the mechanical behavior of a contact zone in a sample composed of salt concrete and a surrounding salt cylinder which was stressed in a triaxial cell. For the modelling work the FEM program CODE_BRIGHT developed by the Polytechnical University in Barcelona was used. Aim was to achieve a maximum porosity of 1.4 % in the joint due to dilatancy.

4.4.1 Model geometry and boundary conditions

The model was created axisymmetric (Fig. 4.8). It consists of a sample, including a salt concrete core, a contact zone and a surrounding salt cylinder, and a steel piston. The height of the sample is 100 mm and its radius is 35 mm. The radius of the sample is composed of 15 mm salt concrete, 15 mm salt cylinder and 5 mm contact zone. However, the thickness of the contact zone is overestimated, as the real thickness is less than 1 mm. The height of the steel piston is 200 mm.
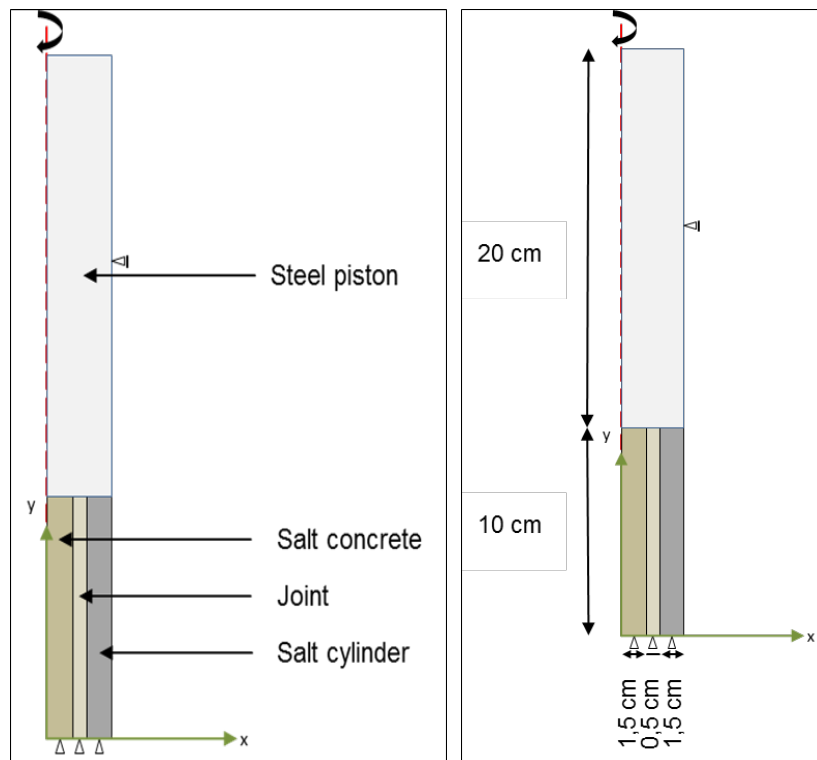
Fig. 4.8 Model geometry of the triaxial test

The salt concrete, the contact zone and the salt cylinder are fixed on the basement, hence all movements in horizontally and vertically direction are disabled. Besides, the steel pistons movement in horizontally direction is also disabled.

The initial temperature is set on 25 °C and the isotropic initial stress is equal to the atmospheric pressure of 0.1 MPa.

The initial porosity value of the steel piston is 0.001, the porosity of the salt concrete is 0.06 and the porosity of the contact zone and the salt cylinder is 0.0035.

The material parameters are shown in Tab. 4.2 – Tab. 4.7. For modelling the contact zone, the material parameters of the salt cylinder, which is composed of rock salt, are adopted. Furthermore, the minimal porosity of the rock salt is set to 0.003 because of the proximity to reality.

Tab. 4.2 Elastic parameters for rock salt

E [MPa]	v [-]	Φ_0 [-]	Φ_{min} [-]
10,000	0.3	0.0035	0.003

Tab. 4.3 Dislocation creep parameters for rock salt

A_A [MPa*s^{-1}]	Q_A [Jm^{-1}]	n [-]
2e-6	54,000	5

Tab. 4.4 Viscoplastic parameters for rock salt

m [-]	Γ_0 [s^{-1}]	Q [Jmol^{-1}]	W_{d0} [-]	a_1 [-]	a_2 [-]	a_3 [-]	a_4 [-]	a_5 [-]	a_6 [-]
8	2e-9	54,000	3.5	2.5	1.8	2.5	0.7	0.02	0.02

Tab. 4.5 Elastic parameters for salt concrete

E [MPa]	v [-]	Φ_0 [-]	Φ_{min} [-]
25,000	0.18	0.06	-

Tab. 4.6 Dislocation creep parameters for salt concrete

A_A [MPa*s^{-1}]	Q_A [Jm^{-1}]	n [-]
0.065e-6	54,000	5

Tab. 4.7 Viscoplastic parameters for salt concrete

m [-]	Γ_0 [s^{-1}]	Q [Jmol^{-1}]	W_{d0} [-]	a_1 [-]	a_2 [-]	a_3 [-]	a_4 [-]	a_5 [-]	a_6 [-]
8	5e-9	54,000	1.7	1.9	0.7	2.5	0.6	0.02	0.02

4.4.2   1st approximation of the contact zone evolution

The first approximation of simulating the mechanical evolution of the contact zone was made by increasing the porosity in the joint due to dilatancy by bringing up a high deviatoric stress. For simplification, the salt concrete was eliminated from the beginning on and the rock salt cylinder is excavated during the modelling, resulting in a more focused consideration on the joint. The modelling steps are presented in the following: .

a) Interval 1 (0.00 - 0.01 days): The joint and the rock salt cylinder are loaded with isotropic stress conditions which are estimated to the atmospheric pressure. The salt concrete is excavated from beginning on (Fig. 4.9).

b) Intervals 2+3 (0.01 - 2 days): The isotropic stress is raised up to 50 MPa and hold on for reaching a damaging of the rock salt and the joint (Fig. 4.10).

c) Intervals 4+5 (2 - 3 days): The radial stress is reduced to 2 MPa for creating a deviatoric stress and activating the dilatant behavior of the rock salt.

d) Intervals 6+7 (3 - 4 days): An isotropic stress state is reached due to the reduction of the axial stress to 2 MPa. The isotropic stress state is needed for the excavation of the rock salt cylinder.

e) Intervals 8+9 (4 - 5 days): The rock salt cylinder is excavated under isotropic stress conditions.

f) Intervals 10+11 (5 - 7 days): The axial stress is increased to 7 MPa creating a deviatoric stress state in the joint. The stress state was chosen because of the compliance with the maximal displacements.
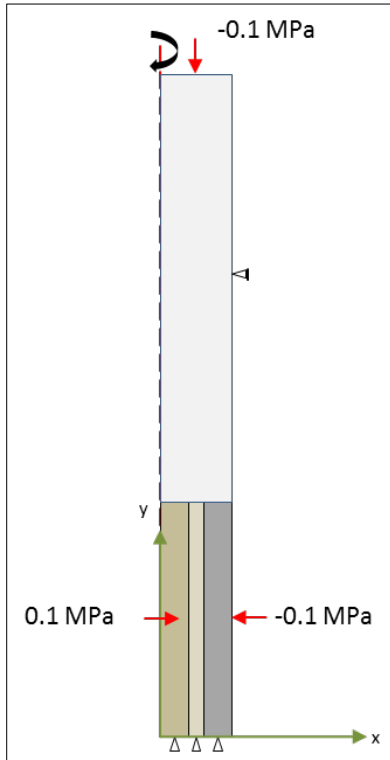
Fig. 4.9 a) Interval 1
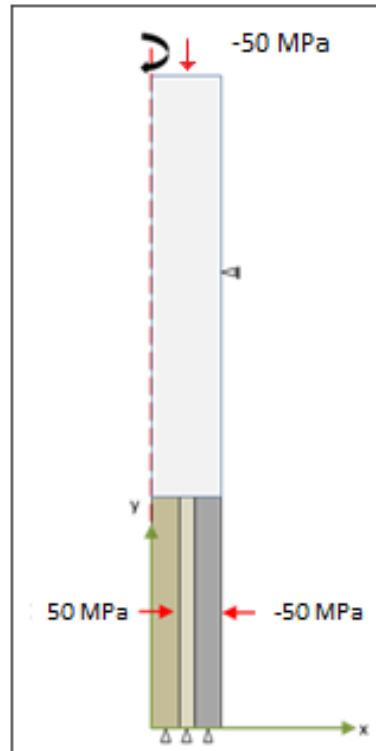
Fig. 4.10 b) Intervals 2+3
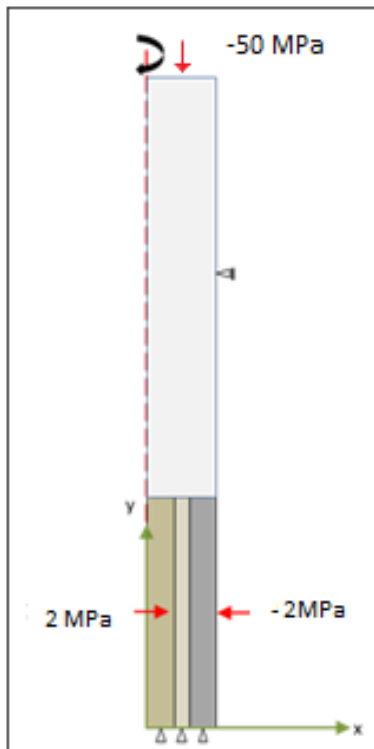
Fig. 4.11 c) Intervals 4+5
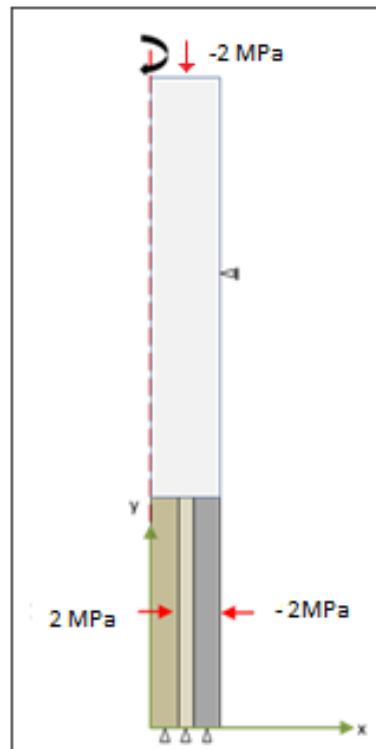
Fig. 4.12 d) Intervals 6+7

42
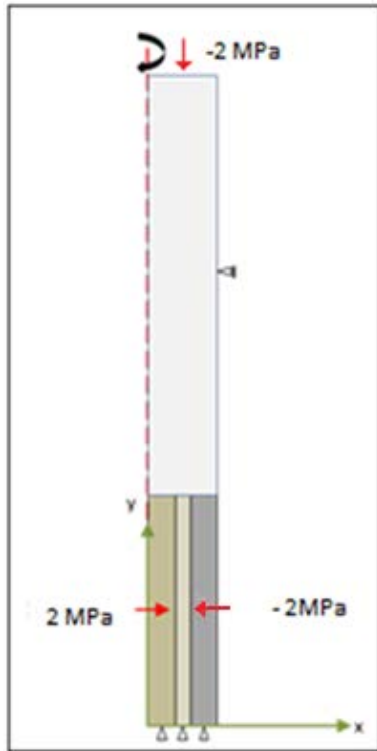
Fig. 4.13 e) Intervals 8+9   **Fig. 4.14** f) Intervals 10+11
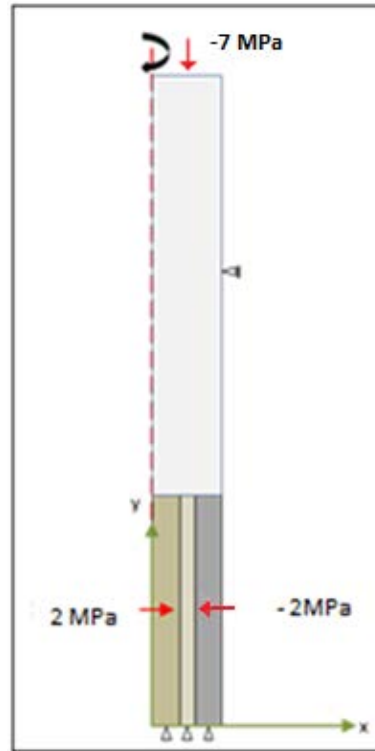
The porosity evolution in the joint is shown in Fig. 4.15. Porosity starts at the initial value of 0.0035 and then decreases rapidly because of the isotropic compression. At 2 days the porosity increases to a value of about 0.00665 which is a result of the deviatoric stress and the dilatant behavior of the rock salt. The joint gets in vertical direction a higher load than in the horizontal direction hence the salt shows an instantaneous volume enlargement due to stress rearrangement, however, with time the porosity is reduced.

At 3 days, there is a fast increase in porosity to a value of 0.00859 resulting from the reduction of axial stress from 50 MPa to 2 MPa which enables a relaxation of the sample. The decrease at 4 days results from the excavation of the rock salt cylinder. Now, the applied force operates on a smaller surface consequently the stresses will be higher and compresses the joint. Due to the rising axial stress at 5 days, the sample gets compacted resulting in a porosity decrease.

The maximal displacements are shown in Fig. 4.16. On account of the plausibility only displacements lower than 5% of the height are permitted. The biggest displacements appear at high deviatoric stress states. In the last part of the

experiment the deviatory stress where the displacements are lower than -0.005 m (= 5 mm = 5 % of the high) had to be determined. With a deviatoric stress of 5 MPa the maximal displacements are accomplished. An increase of the deviatoric stress would result in displacements which are not plausible.

The evolution of stresses in the middle of the joint is shown in Fig. 4.17. The green line represents the radial stress and the red line shows the axial stress evolution. The initial value of both stresses is equal to the atmospheric pressure. Next, the isotropic stress is increased to 50 MPa, however, the axial stress is slightly higher resulting from the smaller surface of the joint and the salt cylinder compared to the steel piston.

After 2.00 days, the radial stress is decreased to 2 MPa and then constant over time. The decrease of the radial stresses produces a deviatoric stress state in the joint resulting in an increase of the axial stress.

At 3 days the axial stress is reduced to 2 MPa reaching an isotropic stress state. At 4.00 days the salt cylinder was excavated leading to an increase in axial stress because of the surface reduction of the sample (only the joint is active).

At 5.00 days the axial stress is increased to 7 MPa on the surface of the steel piston, resulting in an axial stress of about 45 MPa in the joint.

For comparison, the stresses on the top of the joint are shown in Fig. 4.18. They are influenced by the transition region between steel piston and joint.

In this modeling the aim of a maximum porosity value of 1.4 % is not achieved. The maximum value of 0.86 % was reached by relaxation of the sample after reducing the stresses to a low isotropic stress state and before the excavation of the rock salt cylinder. After the excavation of the salt cylinder the porosity decreases by compaction. By raising up the deviatory stress in the end of the modelling the displacements would become a non-realistic value. This first approximation was not suitable to represent the mechanical behavior of the joint.
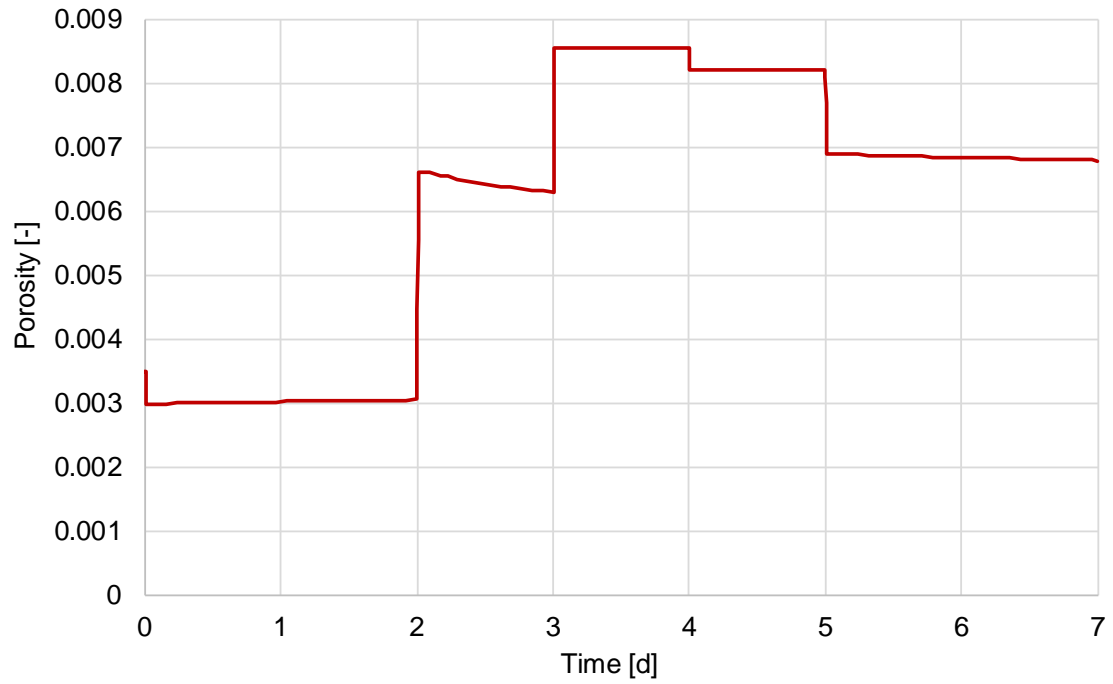
Fig. 4.15   Porosity evolution in the middle of the joint
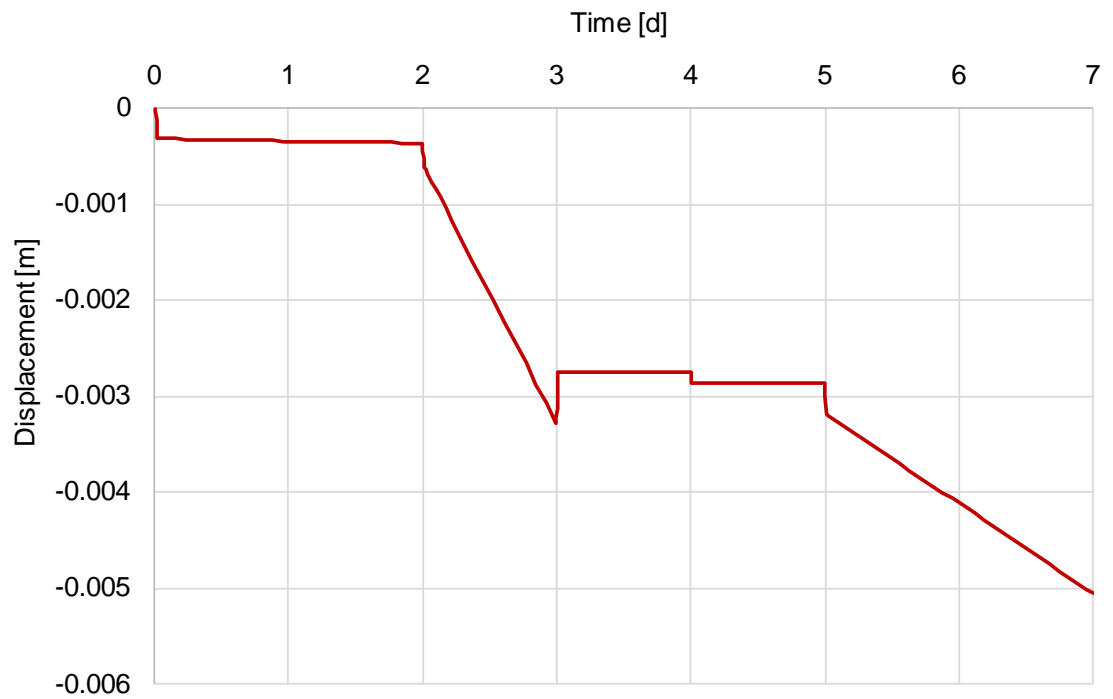
Fig. 4.16   Maximal displacement of the joint
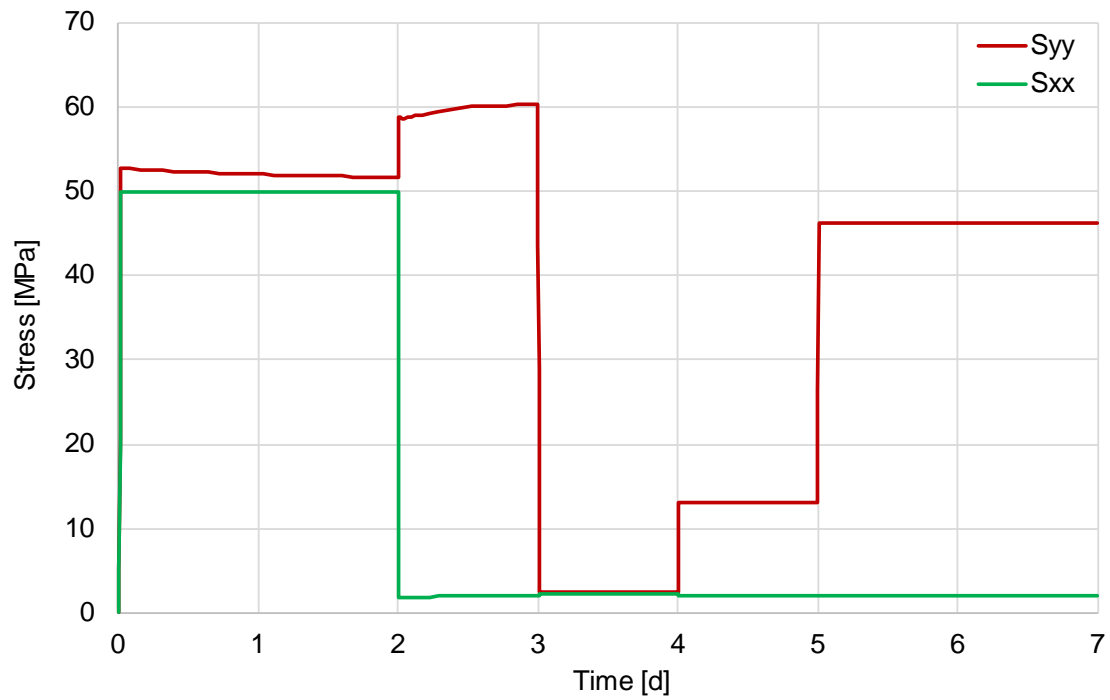
Fig. 4.17   Stress evolution in the middle of the joint
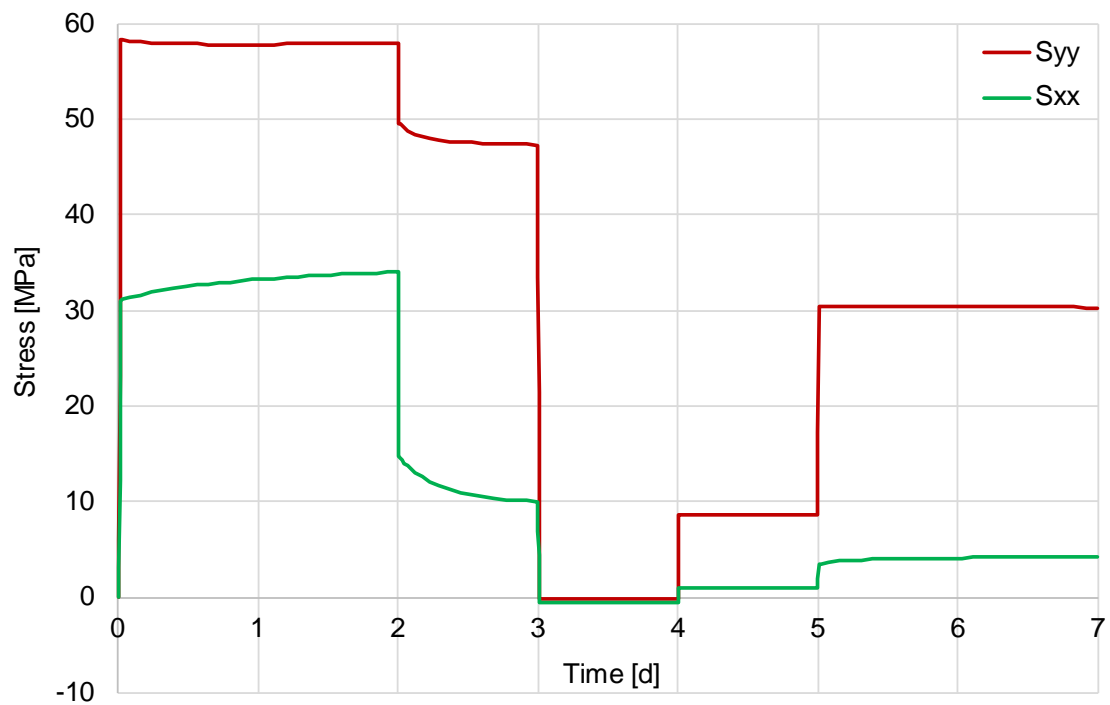
Fig. 4.18   Stress evolution on the top of the joint

4.4.3   2nd approximation of the contact zone evolution

To understand the influence of initial porosity on the mechanical behavior of the joint, the value was changed, however, the other material parameter and the interval data are adopted from the first approximation modelling.

The first chosen initial value for the porosity was 0.5 %, then the value is raised up gradually to 0.7 %, 1 %, 1.2 %, 1.4 % and 1.5 %. In the following, only the results of 0.5 % and 1 % are shown.

For the verification of a possible influence of the rock salt cylinder porosity on the joint, comparative modellings were done. The results show no differences between modellings with equal porosities in the joint and salt cylinder and diverse porosities in the both materials. In the following, only the porosity of the joint is changed.

Fig. 4.19 shows the porosity evolution in the joint with an initial porosity of 0.5 %. By comparing these results with the porosity evolution of the first approximation (Fig. 4.16), no differences, except the initial porosity, can be determined.

Fig. 4.20 shows the porosity evolution with an initial porosity of 1 %. By increasing the isotropic stress state from 2 MPa to 50 MPa, the porosity decreases rapidly to a minimum value of 0.00394 which is higher than in the first approximation modelling (Fig. 4.16) and higher than the fixed minimum porosity. This leads to the conclusion, that the joint is not totally damaged. Both porosity evolutions show the same trend but differ in the maximum porosity. By increasing the initial porosity to 1 %, a maximum porosity during the experiment of 0.0094 is reached, which is slightly higher than the comparative value, however, smaller the initial one.

The increase of initial porosity is not constructive for reaching the modelling aim.
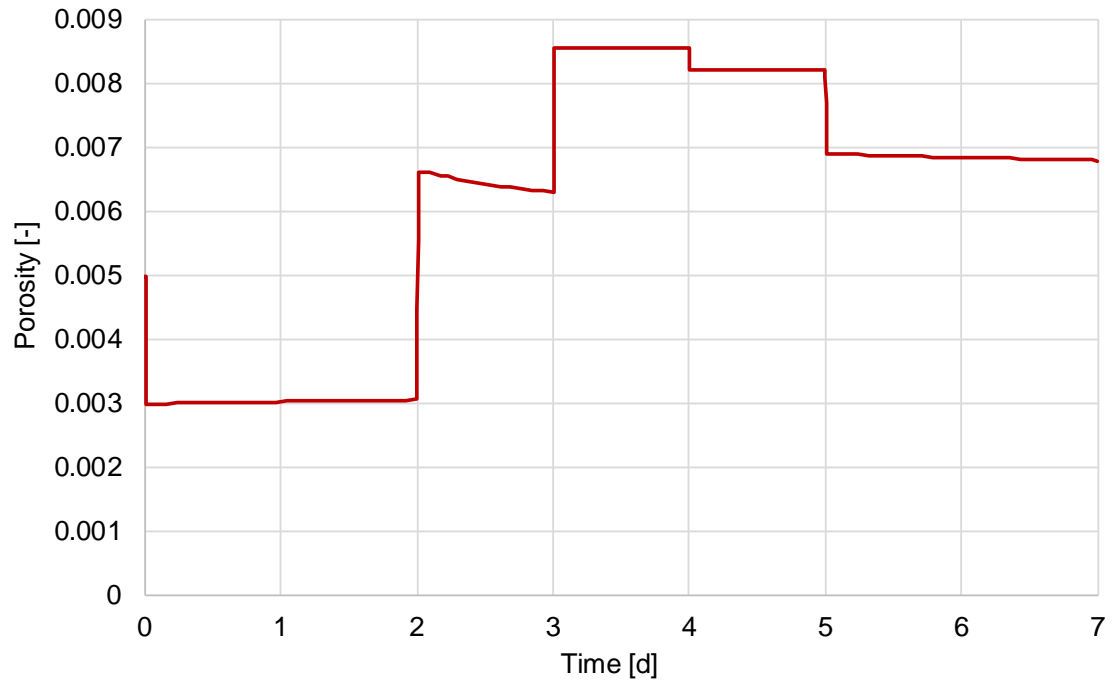
Fig. 4.19   Porosity evolution in the middle of the joint, initial porosity = 0.5 %
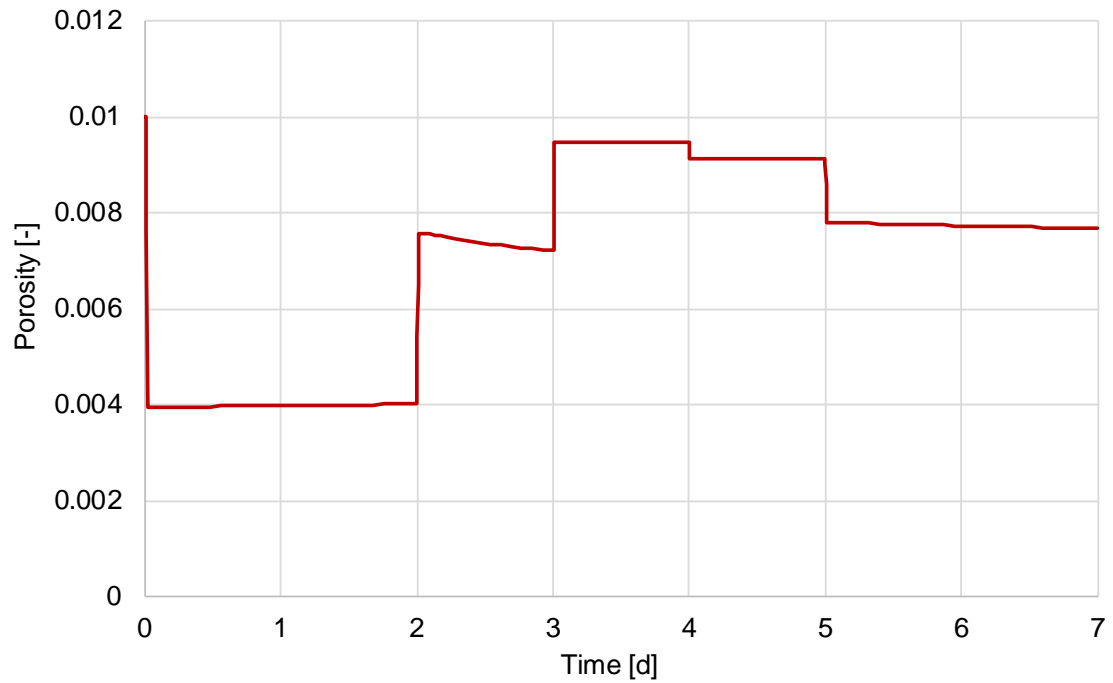
Fig. 4.20   Porosity evolution in the middle of the joint, initial porosity = 1 %

48

4.4.4   3rd approximation of the contact zone evolution

Another approach for increasing the porosity in the joint is to damage the joint and the salt cylinder with a gradually increase of the stress state. Therefore, comparative modellings with different stress states were done. The maximal porosity was reached in a modelling with an isotropic stress state of 75 MPa. Although this value is not reasonable, the results are shown in the following:

The loading history refers to the first approximation:

a) Interval 1 (0.00 - 0.01 days): The joint and the rock salt cylinder are loaded with isotropic stress conditions which are estimated to the atmospheric stress. The salt concrete is excavated from beginning on, Fig. 4.21.

b) Intervals 2+3 (0.01 - 2 days): The axial and the radial stress are raised up to 75 MPa, for reaching an isotropic stress state for damaging the sample through compaction, Fig. 4.22.

c) Intervals 4+5 (2 - 3 days): The radial stress is reduced to 2 MPa for creating a deviatoric stress which leads to an increase in porosity due to dilatancy, Fig. 4.23.

d) Intervals 6+7 (3 - 4 days): The axial stress is reduced to 2 MPa, creating an isotropic stress level which is needed for the excavation of the joint in the next step, Fig. 4.24.

e) Intervals 8+9 (4 - 5 days): The joint is excavated and the stress is hold constant over time, Fig. 4.25.
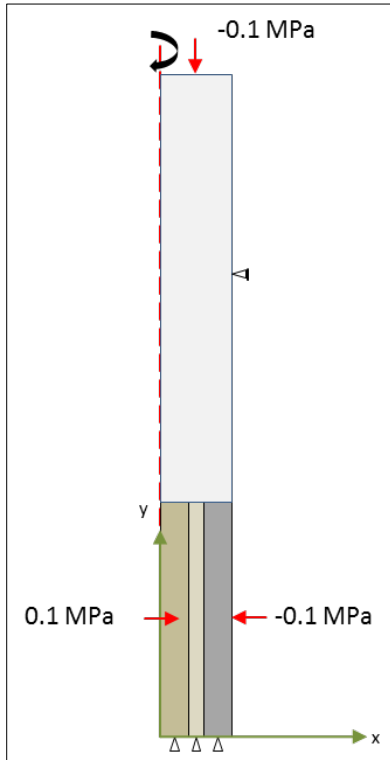
Fig. 4.21 a) Interval 1
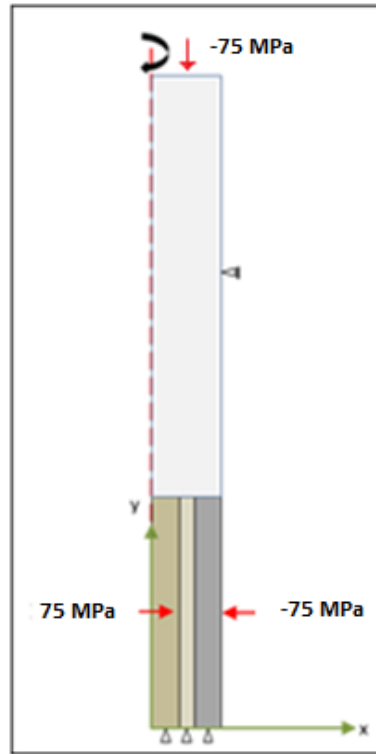
Fig. 4.22 b) Intervals 2+3
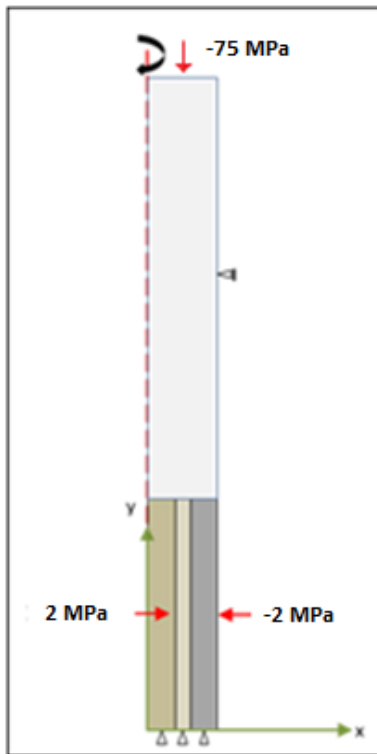
Fig. 4.23 c) Intervals 4+5
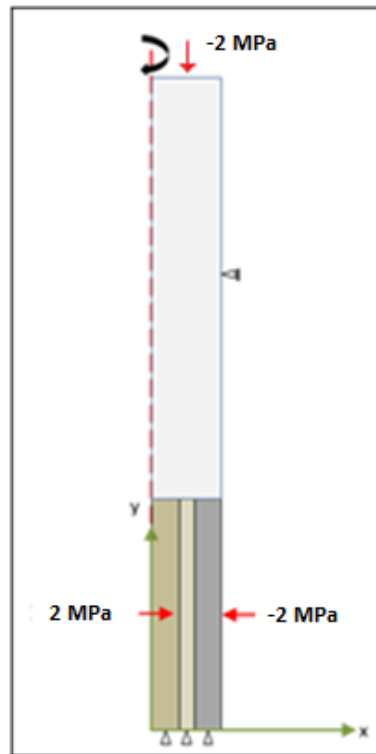
Fig. 4.24 d) Intervals 6+7
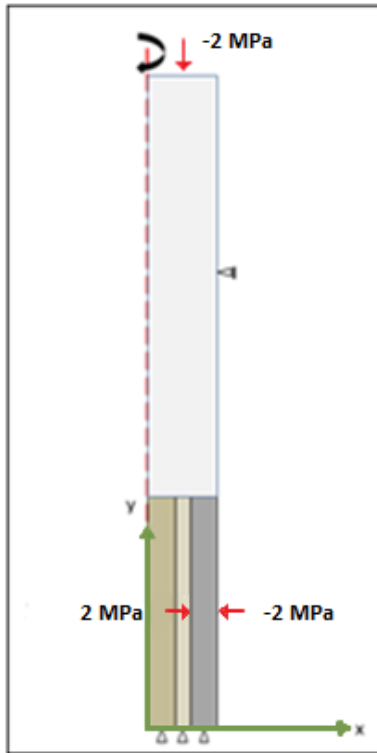
Fig. 4.25 e) Intervals 8+9

The porosity evolution in the joint is shown in Fig. 4.26. It starts with the initial porosity of 0.0035 and is then reduced to minimum porosity because of compaction due to the high stress level. At day 2 the deviatoric stress is increased, resulting in dilatant behavior of the salt and following in a rise in porosity to 0.009. After the instantaneous increase the porosity starts to decrease with time. At 3 days the axial stress is reduced, so that the sample is loaded by an isotropic stress level of 2 MPa. Due to relaxation, the porosity rises to a maximal value of 1 %. The joint is excavated after 4 days, the values after this time are extrapolations.

Fig. 4.27 shows the stress evolution in the middle of the joint. After 0.01 days, the axial and radial stress is increased to 75 MPa. Here also, the resulting axial stress in the joint is slightly higher than the radial stress because the surface of the sample is smaller than the surface of the steel piston, where the stress acts. After 2 days the radial stress is reduced to 2 MPa, creating a deviatoric stress state. For creating an isotropic state for the excavation of the joint, the axial stress is

decreased to 2 MPa after 3 days. The joint was excavated after 4 days, the following values are extrapolated.

By comparing the displacements of this modelling with the results of the first modelling approximation, differences could be determined. According to Fig. 4.28 there are only small displacements during the compaction phase of the sample by an isotropic stress.

After 2 days the deviatoric stress is increased resulting in an rise of displacements. The maximum value is 0.0232 m which correlates 23.2 % of the height.

Bringing up an isotropic stress state of 2 MPa after 3 days results in a relaxation of the sample which is presented by the degeneration of displacements.
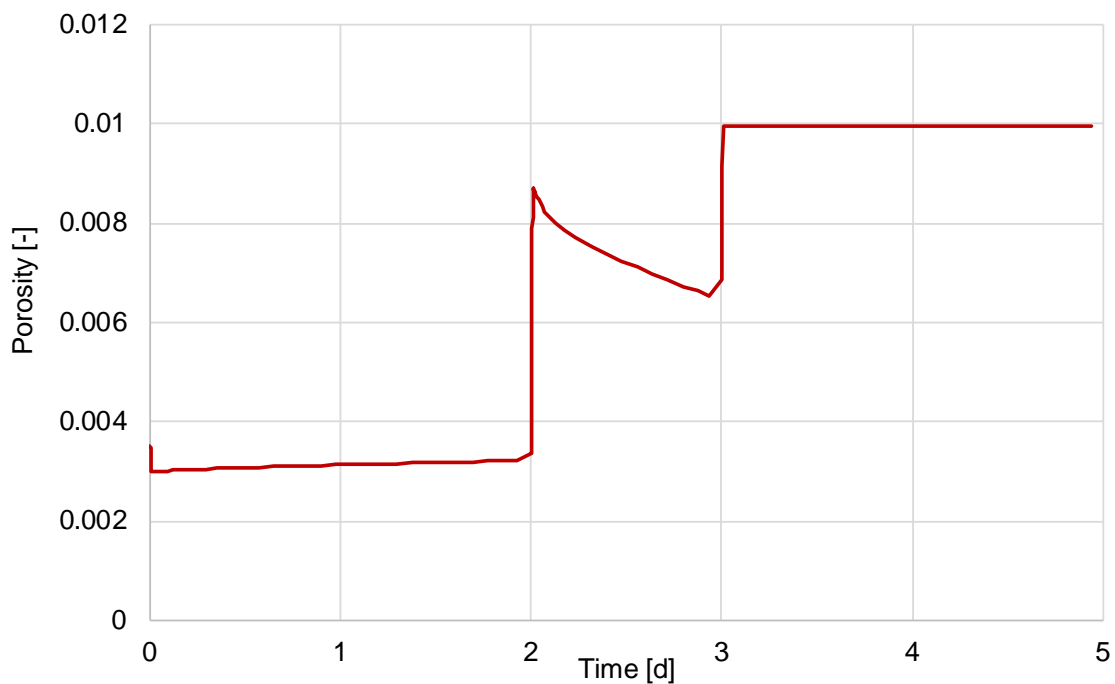
Fig. 4.26 Porosity evolution in the middle of the joint
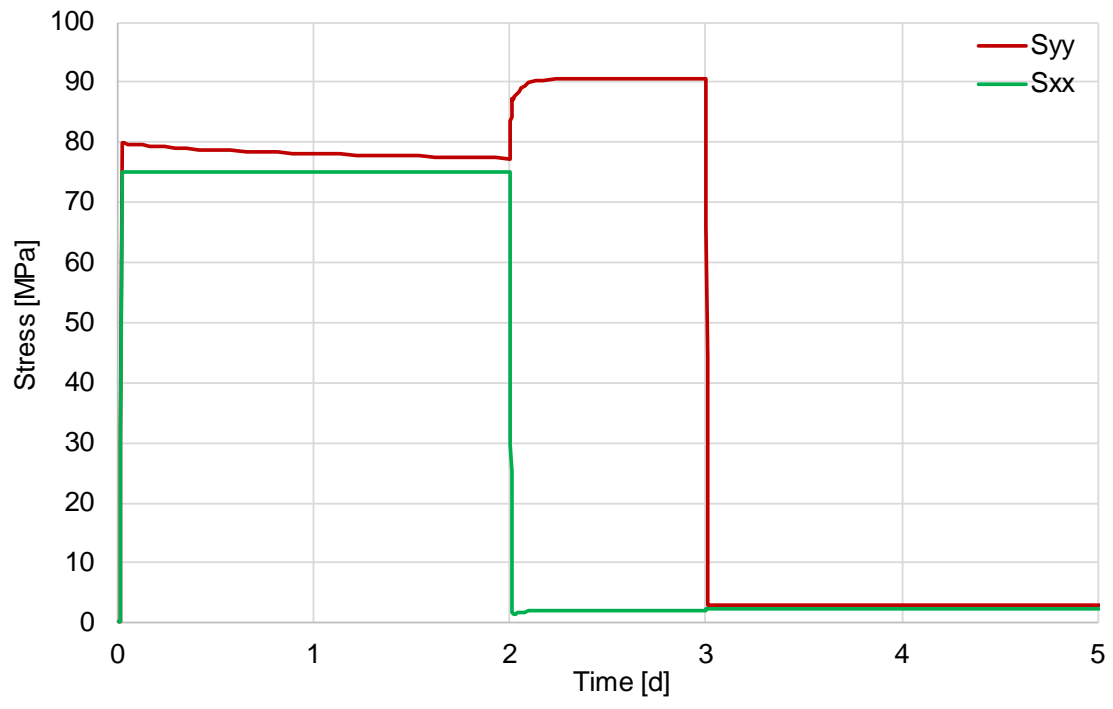
Fig. 4.27 Stress evolution in the middle of the joint
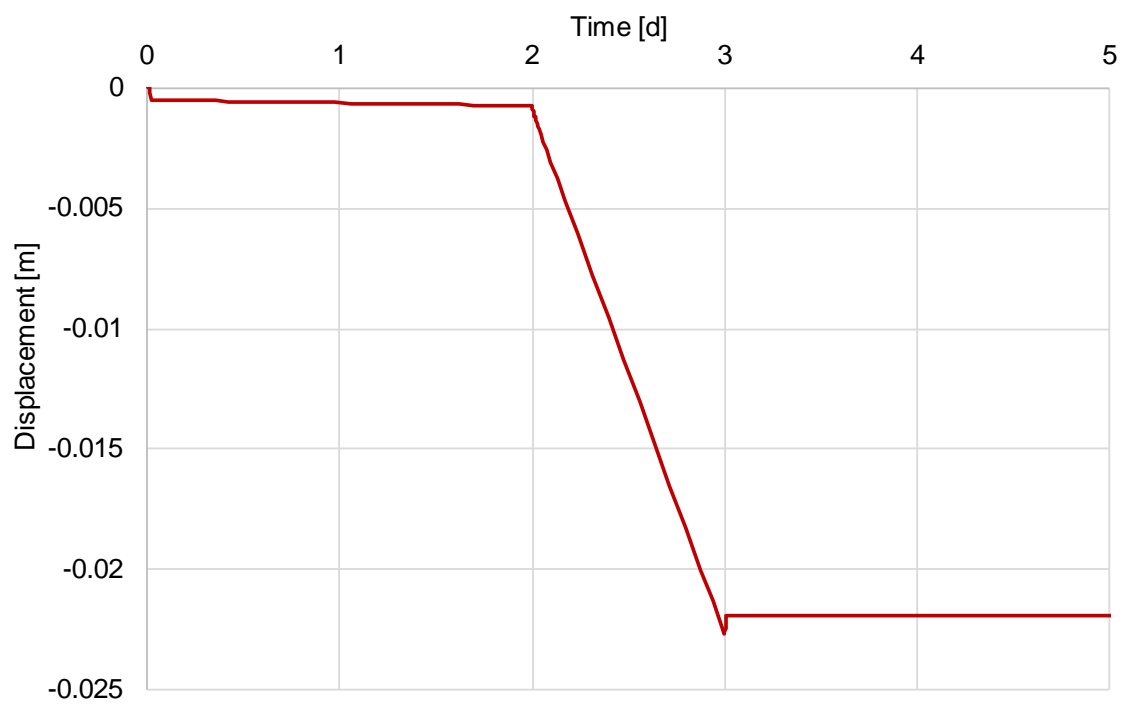
Fig. 4.28 Maximal displacements in the joint

In the following, the evolutions of porosity and stress in the rock salt cylinder are presented. Fig. 4.29 shows the porosity evolution in the middle of the salt cylinder. It starts with the initial porosity of 0.0035 and is then decreased rapidly due to the compaction reaching the minimal porosity of 0.003. When increasing the deviatoric stress after 2 days, the porosity increases because of the rock salts dilatant behavior. With time, the porosity starts to decrease under the deviatoric stress. After 3 days the isotropic stress, needed for the excavation of the joint, is adjusted, leading to a relaxation and an increase in porosity. The excavation of the joint takes place after 4 days, leading to a decrease in porosity.

The evolutions of stresses are shown in Fig. 4.30, where the red graph represents the axial stress and the green one represents the radial stress. For the compaction of the sample, the isotropic stress state is increased from atmospheric pressure to 75 MPa. Because of the samples smaller surface compared to the steel pistons, the resulting axial stress in the salt cylinder is slightly higher. The reduction of the radial stress after 2 days leads to a low decrease in axial stress due to stress rearrangements.

After 3 days, an isotropic stress state of 2 MPa is adjusted. Around 4 days, there is a slight deviation which is shown more detailed in Fig. 4.31. This deviation results from the excavation of the joint which leads to an increase in an increase of axial strains and a decrease in radial strains.

Because the displacements of the rock salt cylinder are equal to those in the joint, they are not presented here.
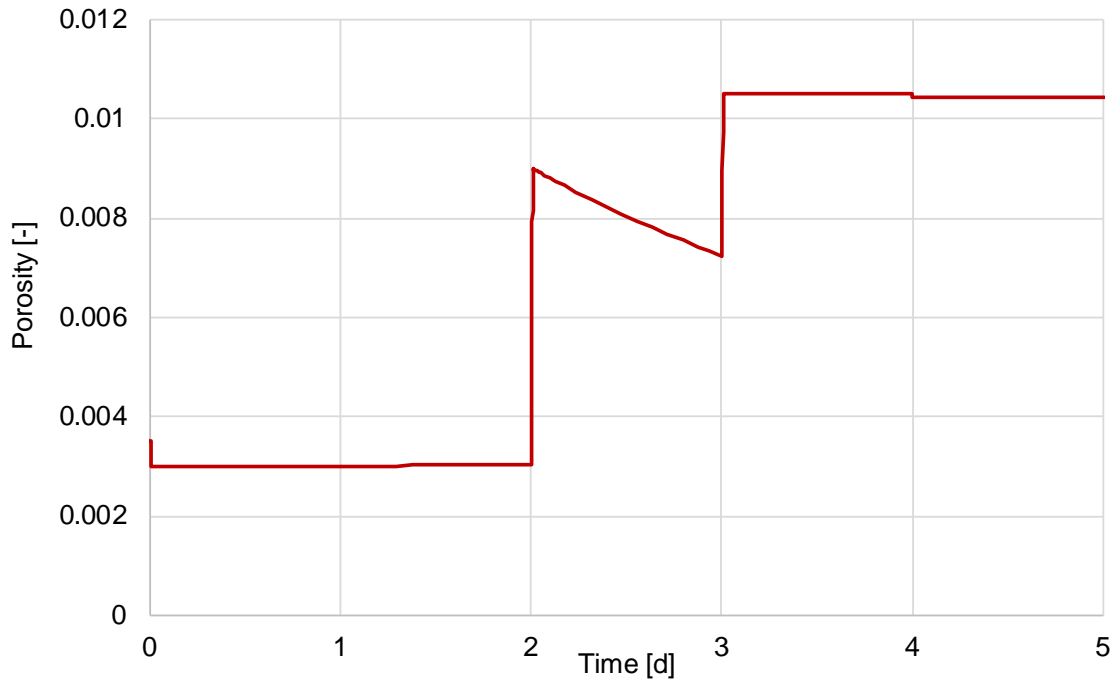
Fig. 4.29   Porosity evolution in the rock salt cylinder
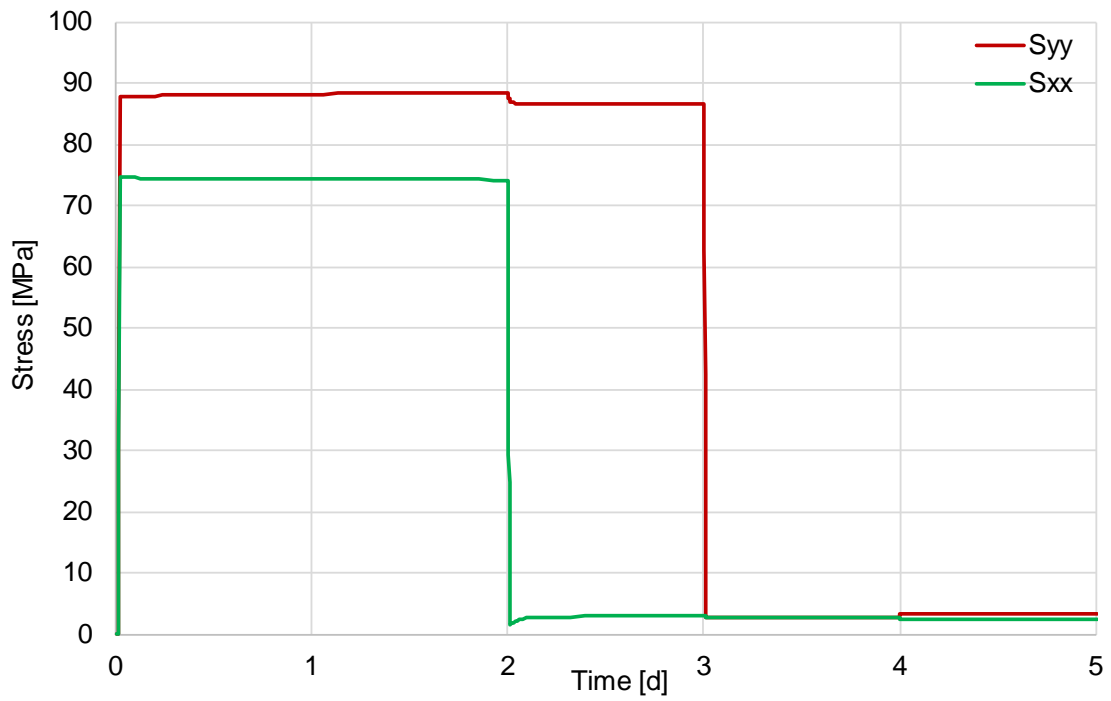
Fig. 4.30   Stress evolution in the rock salt cylinder
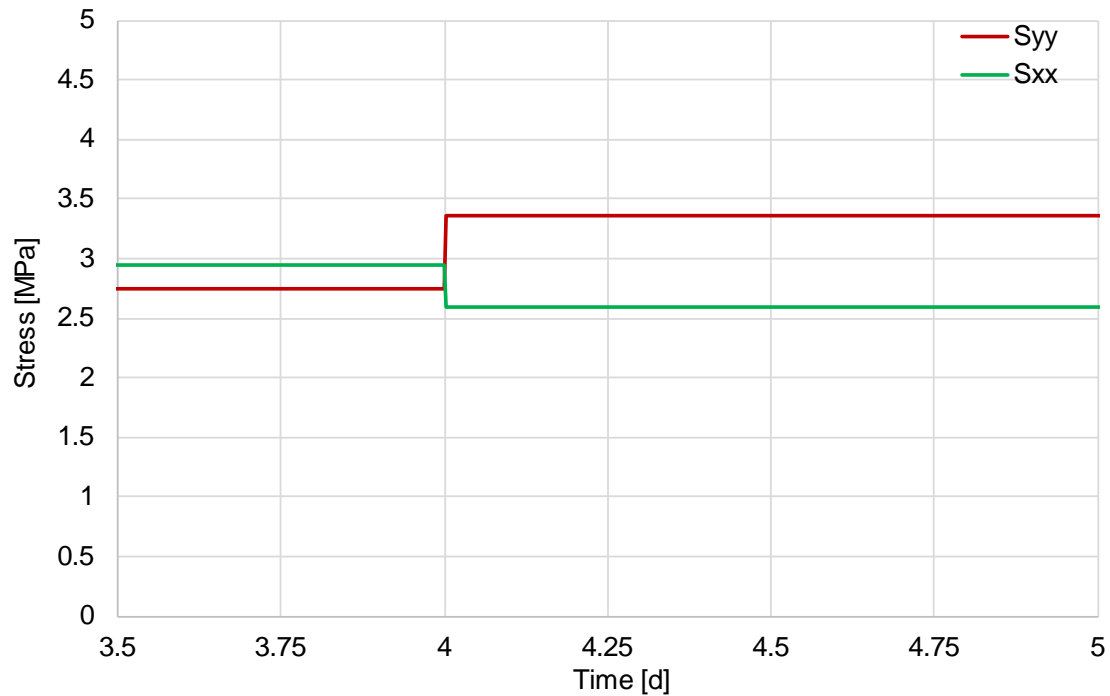
Fig. 4.31   Stress evolution in the rock salt cylinder, zoomed detail

The joint porosity reaches a value of 1 % in this approximation modelling which is higher than in the first approximation. However, as mentioned in the beginning of this subchapter, the question of plausibility has to be answered. The maximum displacement in the joint and in the rock salt cylinder is about 2 cm which correlates to 23 % of the height, however, realistic values for the displacement are in maximum about 5 % of the sample height. This modelling approach is not suitable for representing the mechanical behavior of the joint.

4.5   Discussion

For the former validation and calibration of the constitutive models and computer codes for the analysis of THM processes in the EDZ in rock salt, GRS performed a number of laboratory experiments on the reference salt (Asse Speisesalz). The combined damage and sealing tests were carried out on salt samples with measurements of deformation and permeability under various stress conditions, serving to calibrate the parameters associated to the models.

Most of the process-level models used by the different project partners for numerical modelling are based on consideration of a continuous medium and the dilatancy concept, which relates damage and self-sealing to pore space increase or decrease, respectively. Although not all problems were solved in detail during the calibration phase, all these models reached an advanced calibration state which allowed using them for the prediction of the laboratory benchmark test.

Model simulation of the tests took place in two steps: In the first step, only the loading history of the tests was provided, and the modelling teams were expected to perform a blind prediction. In the second step, the measured sample responses in terms of strains and permeability were distributed and an interpretation modelling phase with improvement of the calibration followed.

CODE_BRIGHT modelled both the benchmark test case and the hollow cylinder with satisfying results for the volumetric strain. Permeability could be modelled well with a cubic law, but the necessary assumptions for fracture spacing and aperture make it difficult to provide a reliable permeability prediction. It is, however, a promising approach because it can be combined with anisotropy and can be applied to unsaturated conditions and gas flow.

The modeling task was to simulate the mechanical behavior of the contact zone between the salt concrete and the salt cylinder with the FEM program CODE_BRIGHT. It is to be achieved by experimental data that the porosity in the joint reaches a value of 1.4 %. Three different approximations were made to capture the experimental data by respective modelling.

At the end, the assumptions made were not in line with realistic boundary conditions (e.g. high deviatoric stress level of 75 MPa, displacements of 23 % of sample height) or initial material parameters.

5   Summary and conclusions

5.1   Scope of the project

GRS is investigating sealing and backfilling materials planned to be utilized in a nuclear repository in a salt formation. The program aims at providing experimental data needed for the theoretical analysis of the long-term sealing capacity of the seal system, including the closing of the contact seam and the recovery of the excavation damaged zone (EDZ) under load and dry or wet conditions.

Since the performance of seals in a rock salt repository is determined by the interaction with the surrounding rock, it is necessary to investigate the system of seal element and rock salt. The critical issue is the recovery of the EDZ. The time scale of recovery will be influenced by the pore fluid. It is known that rock salt deforms more readily in the presence of moisture because pressure solution and redeposition processes are operative. Therefore, a partial saturation of pore space may result in a much faster EDZ recovery. On the other hand, at full saturation a positive pore pressure might develop which reduces compressive stress and hinders recompaction of dilated salt.

So, with respect to EDZ evolution, the following three scenarios are conceivable:

i.   There is no contact between the EDZ and brine/vapor,

ii. There is brine/vapor flow into the sealing system, as a result the EDZ pore space will be partially saturated,

iii. The EDZ or/and the sealing system is nearly fully saturated, as a result to viscous deformation processes positive pore pressures can evolve.

While there is extensive knowledge existing in Germany on long-term rock salt behavior /WIE 10/ for the dry case (i), the material behavior of rock salt in contact with moisture/brine is only known qualitatively. What is missing here is a clear database coming from well-defined experimental investigations on the long-term

recompaction behavior of damaged rock salt itself and in interaction with the seal system, featuring the presence of moisture/brine according to case (ii) and (iii).

To demonstrate hydro-mechanical material stability under representative load scenarios, the impact of the EDZ and the sealing capacity of the seal system, a comprehensive laboratory testing program is carried out. The focus of the work is not on the observation of the saturation process and the derivation of two-phase flow parameters, but on a systematic investigation of the material behavior leading to EDZ recompaction and closure of a potentially conductive contact seam. It is meant to result in a set of material parameters needed to treat the process in a numerical way.

5.2 Results from experimental investigations

The interaction with sealing materials is simulated in laboratory tests by using hollow cylinders of salt equipped with a central concrete seal in isostatic cells. The experimental set-up was applied to eight combined samples, varying the confining stress with time. In general, this procedure resulted in a decrease of permeability in all combined samples. It can be summarized that reduction of per-meability needed more time in samples with a higher initial permeability. Hence, the accuracy of preparation of the salt concrete core and the rock salt cylinder in the turning machine influenced significantly the initial permeability of the com-bined samples. This finding supports the assumption that the contact seam is the primary pathway for solutions.

The influence of the confining stress on the evolution of hydraulic conductivity of the contact seam did not follow a consistent pattern. Therefore, further investiga-tions on combined samples with low initial permeability are needed. Probably, the increased confining stress accelerated the decrease of permeability.

Furthermore, a pilot test with a pre-damaged salt concrete sample was performed in order to check whether the measurement technique for fluid back pressures at inlet and outlet valves was suitable. For that purpose, that the sealing system is nearly fully saturated, and as a result to viscous deformation processes, positive

pore pressures can evolve with a certain influence on the sample permeability. The results of the pilot test clearly showed a decreasing fluid permeability with time. The process of decreasing permeability stops when positive pore pressures evolve.

However, these results showed only a first characteristic trend that should be confirmed by systematic investigations on combined samples.

5.3 Results from numerical modelling

For the former validation and calibration of the constitutive models and computer codes for the analysis of THM processes in the EDZ in rock salt, GRS performed a number of laboratory experiments on the reference salt (Asse Speisesalz). The combined damage and sealing tests were carried out on salt samples with measurements of deformation and permeability under various stress conditions, serving to calibrate the parameters associated to the models.

Most of the process-level models used by the different project partners for numerical modelling are based on consideration of a continuous medium and the dilatancy concept, which relates damage and self-sealing to pore space increase or decrease, respectively. Although not all problems were solved in detail during the calibration phase, all these models reached an advanced calibration state which allowed using them for the prediction of the laboratory benchmark test.

Model simulation of the tests took place in two steps: In the first step, only the loading history of the tests was provided, and the modelling teams were expected to perform a blind prediction. In the second step, the measured sample responses in terms of strains and permeability were distributed and an interpretation modelling phase with improvement of the calibration followed.

CODE_BRIGHT modelled both the benchmark test case and the hollow cylinder with satisfying results for the volumetric strain. Permeability could be modelled well with a cubic law, but the necessary assumptions for fracture spacing and aperture make it difficult to provide a reliable permeability prediction. It is,

however, a promising approach because it can be combined with anisotropy and can be applied to unsaturated conditions and gas flow.

The modeling task was to simulate the mechanical behavior of the contact zone between the salt concrete and the salt cylinder with the FEM program CODE_BRIGHT. It is to be achieved by experimental data that the porosity in the joint reaches a value of 1.4 %. 3 different approximations were made to capture the experimental data by respective modelling. At the end, the assumptions made were not in line with realistic boundary conditions (e.g. high deviatoric stress level of 75 MPa) or initial material parameters.

References

/BEC 04/   Bechthold, W., E. Smailos, S. Heusermann, W. Bollingerfehr, B. Bazargan Sabet, T. Rothfuchs, P. Kamlot, J. Grupa, S. Olivella, F.D. Hansen. 2004. Backfilling and Sealing of Underground Repositories for Radioactive Waste in Salt (BAMBUS-II Project). EUR 20621, Commission of the European Communities.

/BMU 10/   Federal Ministry for the Environment, Nature Conservation, Building and Nuclear Safety (BMU): Safety Requirements Governing the Final Disposal of Heat-Generating Radioactive Waste. Technical Report, 2010.

/CRI 02/   Cristescu, N. D. New trends in rock mechanics, To the beginning of the third Millenium, International Applied Mechanics, Vol. 38, No. 1, 2002.

/CZA 15/   Czaikowski, O., Wieczorek, K., Hertes, U. 2015. Sealing capacity of a seal system in rock salt –Hydraulic impact of the EDZ long-term evolution. 49th US Rock Mechanics / Geomechanics Symposium ARMA 2015, 28 June- 1 July 2015, San Francisco, CA, USA.

/CZA 16/   Czaikowski, O.; Dittrich, J.; Hertes, U.; Jantschik, K.; Wieczorek, K.; Zehle, B. 2016. Development of mechanical-hydraulic models for the prediction of the long-term sealing capacity of concrete based sealing materials in rock salt (LASA), Final Report, **GRS-432**, Gesellschaft für Anlagen- und Reaktorsicherheit (GRS) mbH.

/DOP 12/   Full-scale demonstration of plugs and seals (DOPAS), 2012, Annex 1: Description of work. Grant agreement no: 323273, Seventh framework programme.

/JAN 18a/   Jantschik, K.; Czaikowski, O.; Hertes, U.; Meyer, T.; Moog, H. C.; Zehle, B. 2018 Development of Chemical-hydraulic Models for the Prediction of Long-term Sealing Capacity of Concretebased Sealing Materials in Rock Salt (LAVA I, II), Final Report, **GRS-493**, Gesellschaft für Anlagen- und Reaktorsicherheit (GRS) mbH.

/JAN 18b/   Jantschik, K., Kulenkampff, J., Moog, H. C. 2018. Investigation of the flow along the contact seam between salt cement and rock salt. Mechanical Behaviour of Salt (SaltMech IX), ISBN 978-0-415-62122-9, Hannover, 2018,

/JOC 08/   Jockwer, N.; Wieczorek, K. 2008. ADDIGAS - Advective and Diffuse Gas Transport in Rock Salt Formations (ADDIGAS). Final Report, **GRS-234**, Gesellschaft für Anlagen- und Reaktorsicherheit (GRS) mbH.

/LAR 13/   Larue, J.; Baltes, B.; Fischer, H.; Frieling, G.; Kock, I.; Navarro, M.; Seher, H. 2013, Radiologische Konsequenzenanalyse. Bericht zum Arbeitspaket 10. Vorläufige Sicherheitsanalyse für den Standort Gorleben. **GRS-289**, Gesellschaft für Anlagen- und Reaktorsicherheit (GRS) mbH.

/MÜL 12/   Müller-Hoeppe, N., Buhmann, D.; Czaikowski, O.; Engelhardt, H.-J.; Herbert, H.-J.; Lerch, C.; Linkamp, M.; Wieczorek, K.; Xie, M. 2012. Integrität geotechnischer Barrieren – Teil 1: Vorbemessung, Bericht zum Arbeitspaket 9.2. Vorläufige Sicherheitsanalyse für den Standort Gorleben, **GRS-287**, Gesellschaft für Anlagen- und Reaktorsicherheit (GRS) mbH.

/OLI 02/Olivella, S., Gens, A.: A constitutive model for crushed salt, Int. J. Numer. Anal. Meth. Geomech.; 26; 719-746, 2002.

/RÜB 16/   Rübel. A., Buhmann, D.: Kindlein, J., Lauke, T. 2016. Performance assessment of sealing systems. Conceptual and integrated modelling of plugs and seals. Final Report, **GRS-415**, Gesellschaft für Anlagen- und Reaktorsicherheit (GRS) mbH.

/WIE 07/   Wieczorek, K., Rothfuchs, T.; Zhang, C.-L.; Spies, Th.; Heemann, U.; Lerch, C.; Keesmann, S.; Pudewills, A.; Kamlot, P.; Grupa, J.; Herchen, K.; Olivella, S.; Spiers, C. 2007: Compilation of existing constitutive models and experimental field or laboratory data for the thermal-hydraulic mechanical (THM) modelling of the excavation disturbed zone (EDZ) in rock salt, European Commission,THERESA project, Deliverable D5, Coordinated by Gesellschaft für Anlagen- und Reaktorsicherheit (GRS) mbH, Braunschweig, Germany, 28 August 2007.

/WIE 08/ Wieczorek, K., Heemann, U.; Lerch, C.; Keesmann, S.; Pudewills, A.; Kamlot, P.; Herchen, K.; Olivella, S.; Spiers, C. 2008. THERESA project, Work Package 3, Deliverable D6 - calibration of thermal-hydraulic-mechanical (THM) models of the excavation disturbed zone (EDZ) in rock salt, Coordinated by Gesellschaft für Anlagen- und Reaktorsicherheit (GRS) mbH, Braunschweig, Germany, 14 April 2008.

/WIE 09/ Wieczorek, K., Grupa, J., Kamlot, P., Keesmann, S., Herchen, K., Heemann, U., Olivella, S., Pudewills, A. 2009, THERESA project, Deliverable D8: Model Application on Laboratory Benchmark Test, Coordinated by Gesellschaft für Anlagen- und Reaktorsicherheit (GRS) mbH, Braunschweig, Germany, 31 August 2009.

/WIE 10/ Wieczorek, K., B. Förster, T. Rothfuchs, C.-L. Zhang, S. Olivella, P. Kamlot, R.-M. Günther, C. Lerch. 2010. THERESA Subproject MOLDAU - Coupled Thermal-Hydrological-Mechanical-Chemical Processes for Application in Repository Safety Assessment. Final Report, **GRS-262**, Gesellschaft für Anlagen- und Reaktorsicherheit (GRS) mbH.

/ZHA 09/ Zhang, C.-L, Wieczorek, K., Rothfuchs, T. 2009, Theresa Project, Work Package 3, Deliverable D7, Laboratory Benchmark Tests on rock salt, Coordinated by Gesellschaft für Anlagen- und Reaktorsicherheit (GRS) mbH, Braunschweig, Germany, 30 March 2009.

Figures

Tables